Molecular Pharmacology Fast Forward. Published on September 28, 2016 as DOI: 10.1124/mol.116.105007
This article has not been copyedited and formatted. The final version may differ from this version.

MOL#105007

Extracellular loop 2 of the adenosine A_1 receptor has a key role in orthosteric ligand affinity and agonist efficacy

Anh T.N. Nguyen, Jo-Anne Baltos, Trayder Thomas, Toan D. Nguyen, Laura López Muñoz, Karen J. Gregory, Paul J. White, Patrick M. Sexton, Arthur Christopoulos, Lauren T. May

Monash Institute of Pharmaceutical Sciences (A.T.N.N., J.B., T.T., L.L.M, K.J.G, P.J.W, P.M.S, A.C., L.T.M), Monash e-Research Centre (T.D.N) and Department of Pharmacology (A.T.N.N, J.B., K.J.G., P.M.S., A.C., L.T.M), Monash University, Victoria, Australia

Molecular Pharmacology Fast Forward. Published on September 28, 2016 as DOI: 10.1124/mol.116.105007
This article has not been copyedited and formatted. The final version may differ from this version.

Running title: Role of extracellular loop 2 on A_1 receptor pharmacology

Corresponding Author

To whom correspondence should be addressed:

Lauren May and Arthur Christopoulos

Drug Discovery Biology and Department of Pharmacology,

Monash Institute of Pharmaceutical Sciences,

Monash University

399 Royal Parade, Parkville,

VIC 3052, Australia

Tel.: (613) 9903-9095

Fax: (613) 9903-9581

E-mail: lauren.may@monash.edu, arthur.christopoulos@monash.edu

Manuscript information:

Number of text pages: 21

Number of tables: 2

Number of figures: 8

Number of references: 64

Number of words in abstract: 200

Number of words in introduction: 732

Number of words in discussion: 1598

Molecular Pharmacology Fast Forward. Published on September 28, 2016 as DOI: 10.1124/mol.116.105007
This article has not been copyedited and formatted. The final version may differ from this version.

Non-standard abbreviations

3xHA-A_1AR, human A_1AR containing an amino terminal triple human influenza hemagglutinin epitope tag; [^{3}H]DPCPX, 8-cyclopentyl-1,3-dipropylxanthine [dipropyl-2,3-^{3}H(N)]; A_1AR, adenosine A_1 receptor; AR, adenosine receptor; CHO, Chinese hamster ovary; DMEM, Dulbecco's Modified Eagle Medium; DOPE, Discrete Optimized Protein Energy; DPCPX, 8-cyclopentyl-1,3-dipropylxanthine; ECL2, second extracellular loop; FBS, fetal bovine serum; GPCR, G protein-coupled receptor; HA, human influenza hemagglutinin; IRI, ischemia reperfusion injury; MD, molecular dynamics; NECA, 5′-*N*-ethylcarbozamidoadenosine; PBS, phosphate buffered saline; PME, particle mesh Ewald; POPC, 1-palmitoyl-2-oleoyl-sn-glycero-3-phosphocholine; SLV 320, *trans*-4-[(2-Phenyl-7*H*-pyrrolo[2,3-*d*]pyrimidin-4-yl)amino]cyclohexanol; TM, transmembrane; UK432097, 6-[2,2-di(phenyl)ethylamino]-9-[(2R,3R,4S,5S)-5-(ethylcarbamoyl)-3,4-dihydroxyoxolan-2-yl]-N-[2-[(1-pyridin-2-ylpiperidin-4-yl)carbamoylamino]ethyl]purine-2-carboxamide; WT, wild-type; ZM241385, 4-(2-[7-amino-2-(2-furyl)-[1,2,4]triazolo- [2,3-a][1,3,5]triazin-5-ylamino]ethyl)-phenol.

Molecular Pharmacology Fast Forward. Published on September 28, 2016 as DOI: 10.1124/mol.116.105007
This article has not been copyedited and formatted. The final version may differ from this version.

Abstract

The adenosine A_1 G protein-coupled receptor (A_1AR) is an important therapeutic target implicated in a wide range of cardiovascular and neuronal disorders. Although it is well established that the A_1AR orthosteric site is located within the receptor's transmembrane (TM) bundle, prior studies have implicated extracellular loop 2 (ECL2) as having a significant role in contributing to orthosteric ligand affinity and signaling for various G protein-coupled receptors (GPCRs). We thus performed extensive alanine scanning mutagenesis of the A_1AR-ECL2 to explore the role of this domain on A_1AR orthosteric ligand pharmacology. Using quantitative analytical approaches and molecular modeling, we identify ECL2 residues that interact either directly or indirectly with orthosteric agonists and antagonists. Discrete mutations proximal to a conserved ECL2-TM3 disulfide bond selectively impacted orthosteric ligand affinity, whereas a cluster of five residues near the TM4-ECL2 juncture influenced orthosteric agonist efficacy. A combination of ligand docking, molecular dynamics simulations and mutagenesis results suggest the orthosteric agonist, 5′-*N*-ethylcarboxamidoadenosine (NECA), binds transiently to an extracellular vestibule formed by ECL2 and the top of TMs 5 and 7, prior to entry into the canonical TM bundle orthosteric site. Collectively, this study highlights a key role for ECL2 in A_1AR orthosteric ligand binding and receptor activation.

Molecular Pharmacology Fast Forward. Published on September 28, 2016 as DOI: 10.1124/mol.116.105007
This article has not been copyedited and formatted. The final version may differ from this version.

Introduction

The adenosine receptor (AR) family of G protein-coupled receptors (GPCRs) consists of four subtypes, the A_1AR, A_{2A}AR, A_{2B}AR, and A_3AR. The A_1AR is widely distributed within the body with high levels found in the central nervous system and peripheral organs (Palmer and Stiles, 1995; Fredholm *et al.*, 2001; Yaar *et al.*, 2004). Preferentially coupled to $G_{i/o}$ proteins, A_1AR stimulation can reduce cardiac and renal ischemia reperfusion injury, atrial fibrillation and neuropathic pain (Fredholm *et al.*, 2001). Further, A_1AR antagonists may be beneficial as potassium-saving diuretics (Jacobson and Gao, 2006; Müller and Jacobson, 2011) and cognition enhancers (Hess, 2001). Consequently, the A_1AR is an attractive therapeutic target and a detailed understanding of ligand binding and function is imperative for this clinically relevant target.

Recently, structures of the human A_{2A}AR co-crystallized with various agonists and antagonists have been solved, providing deep insight into the orthosteric ligand binding region (Jaakola *et al.*, 2008; Lebon *et al.*, 2011; Xu *et al.*, 2011; Doré *et al.*, 2011; Congreve *et al.*, 2012; Hino *et al.*, 2012; Liu *et al.*, 2012; Lebon *et al.*, 2015). These crystal structures suggest that both helical transmembrane (TM) domains and extracellular loops (ECLs) contribute to the geography of the orthosteric pocket. In particular, an integral role for the helical region of ECL2 was highlighted, with Phe168 and Glu169 in this loop forming a π-stacking interaction and hydrogen bonding, respectively, with both antagonist and agonists.

Previous homology modeling and mutagenesis studies suggested that the A_1AR orthosteric binding pocket is located within the TM bundle, with key roles attributed to residues L88$^{3.33}$, T91$^{3.36}$, Q92$^{3.37}$ and T277$^{7.42}$ (Townsend-Nicholson and Schofield, 1994; Rivkees *et al.*, 1999). However ECL2, a region with high sequence variability across the adenosine receptor subtypes, has also been implicated in A_1AR orthosteric agonist and antagonist pharmacology (Olah *et al.*, 1994). Similarly, an emerging picture of the contribution of ECL2 in orthosteric ligand recognition, and even the

Molecular Pharmacology Fast Forward. Published on September 28, 2016 as DOI: 10.1124/mol.116.105007
This article has not been copyedited and formatted. The final version may differ from this version.

ability of GPCRs to transition between multiple functional states, has been more broadly suggested for other AR subtypes and family A GPCRs, including the A_{2A}AR, A_3AR, cannabinoid receptor 1, M_2 and M_3 muscarinic acetylcholine receptors, rhodopsin, β-adrenoceptors, dopamine receptors, chemokine receptor 4 and V_{1a} vasopressin receptor (Olah *et al.*, 1994; Kim *et al.*, 1996; Howl and Wheatley, 1996; Gao *et al.*, 2002; Shi and Javitch, 2004; Avlani *et al.*, 2007; Scarselli *et al.*, 2007; Gregory *et al.*, 2010; 2012; Sabbadin *et al*., 2015). In particular, ECL2 residues in the area adjacent to the highly conserved disulfide-bonding cysteine appear to play a key role in agonist binding and function at family A GPCRs (Wheatley *et al.*, 2012). At the human A_{2A}AR, glutamate residues in ECL2 have also been suggested to be involved in orthosteric ligand recognition (Kim *et al.*, 1996). Furthermore, a recent seminal study using unbiased long time-scale molecular dynamics (MD) simulations highlighted a role for ECL2 in entry and egress of β-adrenoceptor orthosteric ligands from the binding pocket. Interestingly, in that study, the trajectory of ligands into the orthosteric pocket involved a metastable state in an extracellular vestibule, delineated by ECL2 and ECL3, prior to entry into the binding pocket within the helical bundle (Dror *et al.*, 2011). It is possible that this paradigm extends to other receptors, and that the residence time a ligand spends in this metastable state prior to engaging the canonical orthosteric site may have implications for receptor activation dynamics and potential allosteric targeting.

Therefore, the aim of the current study was to establish the role of the A_1AR-ECL2 in orthosteric ligand binding and function using a combination of mutagenesis, quantitative analytical pharmacology and molecular modeling. Complete alanine scanning of ECL2 residues was performed and the effects on orthosteric ligand affinity and efficacy quantified using radioligand binding and cAMP accumulation assays. Interpretation of mutagenesis data was facilitated by ligand docking into A_1AR homology models based on agonist and antagonist bound A_{2A}AR crystal structures followed by MD simulations. Ligand docking poses were evaluated by identification and mutational validation of novel ligand-receptor interactions within the A_1AR. Collectively, our

Molecular Pharmacology Fast Forward. Published on September 28, 2016 as DOI: 10.1124/mol.116.105007
This article has not been copyedited and formatted. The final version may differ from this version.

results demonstrate a key role for ECL2 in orthosteric ligand binding and A_1AR activation. We propose that ECL2, together with the top of TM5 and 7, forms an extracellular vestibule that is recognized by NECA (5′-*N*-ethylcarboxamidoadenosine) and facilitates the transition of this agonist into the orthosteric pocket within the transmembrane bundle. This vestibule may also represent a target for recognition of the A_1AR by allosteric ligands.

Molecular Pharmacology Fast Forward. Published on September 28, 2016 as DOI: 10.1124/mol.116.105007
This article has not been copyedited and formatted. The final version may differ from this version.

Materials and Methods

Materials

Chinese hamster ovary (CHO) Flp-In™ cells, Dulbecco's modified Eagle's medium (DMEM) and hygromycin B (Hygrogold™) were purchased from Invitrogen (Carlsbad, CA). Fetal bovine serum (FBS) was purchased from ThermoTrace (Melbourne, VIC, Australia). The Quikchange II™ site-directed mutagenesis kit was purchased Agilent (La Jolla, CA). AlphaScreen™ reagents, OptiPhase Supermix™ scintillation cocktail and [^{3}H]DPCPX (8-cyclopentyl-1,3-dipropylxanthine, [dipropyl-2,3-^{3}H(N)]; specific activity, 120 Ci/mmol) were obtained from PerkinElmer Life Sciences. Primers were purchased from GeneWorks (Hindmarsh, SA, Australia). All other reagents were purchased from Sigma-Aldrich or Tocris and were of analytical grade.

Receptor Mutagenesis

Mutations were introduced into the coding sequence of the human A_1AR containing an amino terminal triple human influenza hemagglutinin (HA) epitope tag (3xHA-A_1AR) in pcDNA3.1+ vector from Missouri S&T cDNA Resource Center (Rolla, MO). Sequence was amplified by PCR using the following primers 5′-GGGGACAAGTTTGTACAAAAAAGCAGGCTTCGCCACCACTTAAGCTTGGTACCACCTG-3′ (N-terminal forward primer including attB, Kozak sequence and N-terminal of pcDNA3.1 site) and 5′-GGGGACCACTTTGTACAAGAAAGCTGGGTCCTAGTCATCAGGCCTCTCTTCTGG-3′ (C-terminal reverse primer including complimentary attB sequence and complimentary C-terminal of A_1AR). The 3xHA-A_1AR coding sequence was subsequently cloned into the Gateway entry vector pDONR201 using the BP clonase enzyme mix (Invitrogen). Alanine amino acid substitutions were performed using oligonucleotides from GeneWorks (Hindmarsh, South Australia) (Supplemental Table 1) and QuikChange II site-directed mutagenesis kits (Stratagene, La Jolla, CA) according to the manufacturer's instructions. Sequences of receptor clones were confirmed by automated sequencing as described previously (May *et al.*, 2007). Receptor clones

Molecular Pharmacology Fast Forward. Published on September 28, 2016 as DOI: 10.1124/mol.116.105007
This article has not been copyedited and formatted. The final version may differ from this version.

were then sub-cloned into the Gateway destination vector pEF5/FRT/V5-DEST using the LR clonase enzyme mix (Invitrogen).

Transfections and Cell Culture

DNA constructs in the pEF5/FRT/V5-DEST destination vector were stably transfected into Flp-In™-CHO cell line as described previously (May *et al.*, 2007). Briefly, Flp-In™-CHO cells were transfected in serum and antibiotic-free DMEM with 0.7 μg of pEF5/FRT/V5-DEST vector containing the wild-type (WT) or mutant 3xHA-A_1AR constructs and 7 μg of pOG44 vector using Lipofectamine 2000 (30 μL/25 cm^2 flask). Flp-In™-CHO cells stably expressing human A_1AR (untagged) were generated previously (Valant *et al.*, 2014). Cells were selected and maintained in DMEM containing 10% FBS and 600 μg/mL hygromycin B in a humidified environment at 37°C in 5% CO_2.

Radioligand binding assay

Cells were seeded at 40,000 cells/well into a transparent 96-well plate and incubated in a humidified environment at 37°C in 5% CO_2. After 8 h, cells were washed with serum free DMEM and maintained in serum free DMEM for approximately 18 h at 37°C in 5% CO_2 before assaying. [^{3}H]DPCPX whole cell saturation binding assays on Flp-In™-CHO cells stably expressing A_1AR constructs were performed at 4°C for 3 h in a final volume of 100 μL HEPES buffer (145 mM NaCl, 10 mM D-Glucose, 5 mM KCl, 1 mM $MgSO_4$, 10 mM HEPES, 1.3 mM $CaCl_2$, 15 mM $NaHCO_3$, pH 7.4) in the absence or presence of increasing concentrations of [^{3}H]DPCPX (0.1 nM-10 nM). [^{3}H]DPCPX whole cell competition binding assays were performed under the same conditions with ~1 nM [^{3}H]DPCPX and increasing concentrations of NECA (0.3 nM-30 μM) or DPCPX (8-Cyclopentyl-1,3-dipropylxanthine; 0.1 nM-10 μM). Nonspecific binding was defined in the presence of 1 μM SLV 320 (*trans*-4-[(2-Phenyl-7*H*-pyrrolo[2,3-*d*]pyrimidin-4-yl)amino]cyclohexanol), a selective A_1AR antagonist (Kalk *et al.*, 2007) . Assays were terminated

Molecular Pharmacology Fast Forward. Published on September 28, 2016 as DOI: 10.1124/mol.116.105007
This article has not been copyedited and formatted. The final version may differ from this version.

by washing twice with 100 μL cold phosphate buffered saline (PBS)/well, followed by the addition of 100 μL OptiPhase Supermix™ scintillation cocktail and bound radioactivity measured using a MicroBeta^2 ™ plate counter (PerkinElmer).

cAMP accumulation assay

Inhibition of forskolin-stimulated cAMP accumulation assays were performed as described previously (Baltos *et al.*, 2016). Briefly, cells were seeded at 20,000 cells/well into a transparent 96-well plate and incubated in a humidified incubator at 37^{o}C in 5% CO_2 overnight. Media was then replaced with stimulation buffer (140 mM NaCl, 5.4 mM KCl, 0.8 μM $MgSO_4$, 0.2 mM Na_2HPO_4, 0.44 mM KH_2PO_4, 1.3 mM $CaCl_2$, 5.6 mM D-glucose, 5 mM HEPES, 0.1% bovine serum albumin, and 10 μM rolipram, pH 7.45) and incubated at 37°C for 30 min. Concentration response assays were performed by subsequent incubation of NECA (10 pM - 10 μM) and 3 μM forskolin for an additional 30 min at 37°C. Detection of cAMP was performed using AlphaScreen® cAMP Assay kits (PerkinElmer; Boston, MA) and fluorescence was measured with an EnVision® plate reader (PerkinElmer; Boston, MA) using standard AlphaScreen™ settings. Agonist concentration-response curves were normalized to the response mediated by 3 μM forskolin (0%) or buffer (100%) alone.

Data Analysis

All data were analysed using GraphPad Prism 6.03 (GraphPad Software, San Diego, CA). Relative receptor expression (B_{max}) and [^{3}H]DPCPX equilibrium dissociation constants (K_A) were determined from saturation binding assays using the following equation:

$$Y = \frac{B_{\max}[A]}{[A]+K_D} + NS[A] \qquad \text{(Equation 1)}$$

Molecular Pharmacology Fast Forward. Published on September 28, 2016 as DOI: 10.1124/mol.116.105007
This article has not been copyedited and formatted. The final version may differ from this version.

where Y is radioligand binding, B_{max} is the total receptor density, [A] is the radioligand concentration, K_D is the equilibrium dissociation constant of the radioligand, and NS is nonspecific radioligand binding.

[^{3}H]DPCPX competition binding curves were fitted to a one-site inhibitory mass action equation:

$$Y = Bottom + \frac{Top - Bottom}{1 + 10^{(X - LogIC_{50})}} \quad \text{(Equation 2)}$$

where Y is the specific binding and IC_{50} is the concentration of ligand that displaces 50% of the radioligand. Top and bottom represent the maximal and minimal binding in the presence of the competitive ligand, respectively. Equilibrium dissociation constant, (K_I) values were subsequently derived from inhibition binding experiments using the Cheng-Prusoff equation (Cheng and Prusoff, 1973):

$$K_I = \frac{IC_{50}}{1 + \frac{[A]}{K_D}} \quad \text{(Equation 3)}$$

NECA concentration-response curves were fitted to the following form of the operational model of agonism (Black and Leff, 1983):

$$Y = basal + \frac{E_m - basal}{1 + \left(\frac{K_A + [A]}{\tau \times [A]} \right)^n} \quad \text{(Equation 4)}$$

where E_m is the maximal system response, A is the agonist concentration, τ is an index of coupling efficiency (efficacy) of the agonist and is defined as R_T/K_E (where R_T is the total concentration of receptors, i.e., B_{max}, and K_E is the concentration of agonist-receptor complex that yields half the E_m), and n is the slope of the transducer function that links occupancy to response; the latter parameter was constrained to be shared across all datasets, as an extra-sum-of-squares (F test) determined that curve fitting was not improved by allowing different transducer slopes for different receptor mutations. K_A values were constrained to their respective K_I values estimated from [^{3}H]DPCPX competition binding studies. To account for effects of the expression level of each of the different mutant receptors on the observed efficacy of each agonist, the B_{max} values determined

Molecular Pharmacology Fast Forward. Published on September 28, 2016 as DOI: 10.1124/mol.116.105007
This article has not been copyedited and formatted. The final version may differ from this version.

from saturation binding were used to normalize the τ values derived from the operational model analysis (Gregory *et al.*, 2010); these values are reported as "corrected τ values", τ_c.

Statistical analysis was performed using a Student's *t*-test or a one-way ANOVA analysis of variance with a Dunnett's post-test as indicated was used to determine statistical differences ($P < 0.05$) where appropriate.

Molecular Modeling

Homology Modeling of the A_1AR

The human A_1AR and A_{2A}AR share approximately 40% sequence identity and therefore A_{2A}R crystal structures are acceptable templates for A_1AR homology models to gain a better understanding of ligand interactions at the A_1AR. The sequence of the human A_1AR was retrieved from the Swiss-Prot database. ClustalX software (Thompson *et al.*, 1997) was used to align the A_1AR sequence with the crystal structures of the antagonist and agonist-bound human A_{2A}AR (PDB ID: 3EML (Jaakola *et al.*, 2008) and 3QAK (Xu *et al.*, 2011) for the inactive and partially active states, respectively). 3D structures of the A_1AR were constructed with MODELLER v9.12 (Eswar *et al.*, 2007). The conserved disulfide bond between residue $C80^{3.25}$ at the top of TM3 and $C169^{ECL2}$ and the ECL3 intra-loop disulfide bond between $C260^{ECL3}$ and $C263^{ECL3}$ present in the template structure were built and maintained as a constraint for geometric optimization. The best structure was selected based on the Modeller DOPE (Discrete Optimized Protein Energy) assessment score and visual inspection. Structures obtained were optimized using the Duan force field (Duan *et al.*, 2003).

Docking of adenosine receptor ligands

Docking of DPCPX and NECA was performed using ICM version 3.8.0 (Molsoft L.L.C., La Jolla, CA). Potential binding sites were predicted using the ICM Pocket Finder algorithm (An *et al.*, 2005; Abagyan and Kufareva, 2009). The docking search boundaries were defined by a box of 30 Å x 30

Molecular Pharmacology Fast Forward. Published on September 28, 2016 as DOI: 10.1124/mol.116.105007
This article has not been copyedited and formatted. The final version may differ from this version.

Å x 30 Å (the region in which 0.5 Å grid energy maps were generated), this size is large enough to encompass the potential orthosteric binding pocket and the extracellular region of the receptor. Docking thoroughness, representing the length of the docking simulation, used default settings. Ligand binding modes were ranked according to ICM score, which is inversely proportional to the number of favorable intermolecular interactions between the docked ligand and the receptor. The docking of each ligand was repeated five times and the conformation with the lowest ICM score selected for subsequent MD simulations.

Molecular Dynamics Simulations

MD simulations of the final complex were carried out with the NAMD2.10 (Phillips *et al.*, 2005) package using the 3-site rigid water TIP3P model, CHARMM27 (MacKerell *et al.*, 1998; Mackerell *et al.*, 2004), and CGenFF (Vanommeslaeghe *et al.*, 2010; Yu *et al.*, 2012) v.3.0.1 force fields as described previously (Aksimentiev *et al.*, 2012; Shonberg *et al.*, 2013). The particle mesh Ewald (PME)(Essmann *et al.*, 1995) method was used to evaluate electrostatic interactions. Each system contains an A_1AR receptor, the ligand, a lipid bilayer containing ~220 1-palmitoyl-2-oleoyl-sn-glycero-3-phosphocholine (POPC) molecules generated using the membrane plugin of the VMD software (v1.9.2) (Humphrey *et al.*, 1996), and ~15800 water molecules. Sodium and chloride ions were added to neutralize the system, with extra NaCl added to reach a final concentration of 150 mM (~35 sodium ions, ~48 chloride ions). Two energy minimization and equilibration periods were performed prior to the MD production run. The first involved energy minimization and a 15 ns equilibration of lipids tails. The second involved energy minimization and a 5 ns equilibration of the whole system, with 10 kcal $mol^{-1}Å^{-2}$ harmonic-position restraints applied to all heavy atoms of the protein and ligands. Subsequently, the production run of the final unconstrained system was performed for 40 ns using a 2 fs integration time step in the NPT ensemble (310K, 1 bar). Coordinates were written to the output trajectory file every 10 ps. VMD v1.9.2 was used for the visualization and analysis of the residue-ligand contacts through the course of each simulation using in-house scripts. The percentage total MD time that residues were involved in hydrogen bonding

Molecular Pharmacology Fast Forward. Published on September 28, 2016 as DOI: 10.1124/mol.116.105007
This article has not been copyedited and formatted. The final version may differ from this version.

and/or found within 3.5 Å of DPCPX or NECA heavy atoms was quantified for each MD simulation. All figures were generated using PYMOL.

Results

The 3xHA-A_1AR has comparable pharmacology to the human A_1AR

In this study, the role of ECL2 residues on agonist binding and function was investigated using human A_1AR constructs with an N-terminal triple HA epitope tag (3xHA-A_1AR). Previous studies on other GPCRs have shown that the addition of an N-terminal HA-tag generally does not interfere with receptor pharmacology (Sromek and Harden, 1998; Leach *et al.*, 2011; Schiedel *et al.*, 2011). To ensure the pharmacology of the 3xHA-A_1AR was equivalent to the untagged human A_1AR, we compared agonist and antagonist affinity estimated between the two constructs. In homologous competition binding studies, the N-terminal 3xHA tag significantly reduced receptor expression (B_{max}) (A_1AR B_{max} = 5343 ± 234.6, 3xHA-A_1AR B_{max} = 2022 ± 155; n = 3 – 6; $P < 0.05$, Student's *t*-test), however, DPCPX affinity was unaffected (A_1AR pK_I = 8.84 ± 0.08, 3xHA-A_1AR pK_I = 8.96 ± 0.11; n = 3 – 6; $P > 0.05$, Student's *t*-test). In heterologous competition binding studies, NECA affinity was also unaffected (A_1AR pK_I = 6.48 ± 0.01, 3xHA-A_1AR pK_I = 6.59 ± 0.04; n = 3 – 44; $P > 0.05$, Student's *t*-test). Therefore despite having decreased cell surface expression, the N-terminal 3xHA epitope tagged human A_1AR has equivalent affinity with the orthosteric ligands to the untagged human A_1AR.

Cell surface expression of human 3xHA-A_1AR ECL2 alanine mutants

The generalized numbering scheme proposed by Ballesteros and Weinstein was used for transmembrane residues (Ballesteros and Weinstein, 1995). Alanine scanning mutations were performed within ECL2 of the A_1AR, with the exception of $C169^{ECL2}$. Residues $C80^{3.25}$ and $C169^{ECL2}$ are predicted to form a conserved disulphide bond, and alanine substitution of $C169^{ECL2}$ has previously been shown to abolish [^{3}H]DPCPX specific binding (Scholl and Wells, 2000;

Molecular Pharmacology Fast Forward. Published on September 28, 2016 as DOI: 10.1124/mol.116.105007
This article has not been copyedited and formatted. The final version may differ from this version.

Martinelli and Tuccinardi, 2008). Single alanine mutations were performed, with the exception of $S150^{ECL2}A$ + $V151^{ECL2}A$ ($SV150^{ECL2}AA$) and $M162^{ECL2}A$ + $G163^{ECL2}A$ + $E164^{ECL2}A$ ($MGE162^{ECL2}AAA$), for which the double and triple mutations were similarly expressed (Fig. 1A). Cell surface expression of each mutant 3xHA-A_1AR stably expressed in Flp-In™-CHO cells was determined from whole cell [^{3}H]DPCPX saturation binding (Fig. 1B, Fig. 2A). No [^{3}H]DPCPX specific binding could be detected at the $F171^{ECL2}A$ mutation, however subsequent detection of the 3xHA tag with an ELISA found that the cell surface expression of the $F171^{ECL2}A$ receptor was not significantly different to that of the WT A_1AR ($P > 0.05$, unpaired t test; Supplemental Fig. 1). Orthosteric ligand affinity is predicted to be significantly influenced by the $F171^{ECL2}A$ mutation as the corresponding residue at the A_{2A}AR, $F168^{ECL2}$, has been previously shown to form a π-stacking interaction with the antagonist ZM241385 (4-(2-[7-amino-2-(2-furyl)-[1,2,4]triazolo- [2,3-a][1,3,5]triazin-5-ylamino]ethyl)-phenol) and agonist NECA in A_{2A}AR crystal structures (Jaakola *et al.*, 2008; Liu *et al.*, 2012). As such, the lack of [^{3}H]DPCPX specific binding observed for $F171^{ECL2}A$ is likely due to a significant decrease in [^{3}H]DPCPX affinity. Of the remaining 25 mutant 3xHA-A_1ARs investigated, 17 mutant 3xHA-A_1AR Flp-In™-CHO cell lines had significantly reduced cell surface receptor expression compared to the WT 3xHA-A_1AR Flp-In™-CHO cell line (Fig. 1B, Supplemental Table 2).

ECL2 alanine substitutions influence A_1AR orthosteric ligand affinity

The affinity of the orthosteric antagonist [^{3}H]DPCPX and orthosteric agonist NECA was determined from whole cell saturation and competition binding assays, respectively (Fig. 2A, Fig. 2B, Table 1). When compared to the WT 3xHA-A_1AR, alanine substitution of multiple residues ($N159^{ECL2}$, $S161^{ECL2}$, $I167^{ECL2}$, $E172^{ECL2}$, $I175^{ECL2}$ and $M177^{ECL2}$) located in the middle to end of ECL2, significantly decreased [^{3}H]DPCPX affinity (pK_D) (Fig. 3A). The same residues had a similar or greater effect on NECA affinity (pK_I) (Fig. 3B), suggesting that these ECL2 residues facilitate, through direct or indirect interactions, the binding of [^{3}H]DPCPX and NECA at the

Molecular Pharmacology Fast Forward. Published on September 28, 2016 as DOI: 10.1124/mol.116.105007
This article has not been copyedited and formatted. The final version may differ from this version.

A_1AR. Three additional ECL2 mutations, W146^{ECL2}A, L149^{ECL2}A and E170^{ECL2}A, had a modest effect on NECA affinity (Fig. 3B, Table1).

ECL2 alanine substitutions influence A_1AR orthosteric agonist efficacy

To investigate the influence of ECL2 on A_1AR agonist efficacy, NECA-mediated inhibition of forskolin-stimulated cAMP accumulation was quantified in WT and mutant 3xHA-A_1AR Flp-In™-CHO cell lines (Fig. 2C). The NECA-mediated inhibition of cAMP accumulation was comparable in the absence and presence of adenosine deaminase, suggesting minimal influence of endogenous adenosine (unpublished results). Furthermore, we have recently demonstrated that the Flp-In™-CHO cell line stably expressing the wild-type A_1AR was not associated with measureable constitutive activity (Vecchio *et al.*, 2016). Similarly, comparison of the cAMP accumulation stimulated by forskolin (3 μM) found no evidence for A_1AR constitutive activity in Flp-In™-CHO cells stably expressing mutant A_1ARs (unpublished results). An operational measure of efficacy (logτ), corrected for relative receptor expression levels, was used to quantify efficacy changes at mutant 3xHA-A_1ARs compared to the WT 3xHA-A_1AR. Negligible NECA-mediated inhibition of cAMP accumulation was observed in the Flp-In™-CHO cell line expressing the 3xHA-A_1AR(F171^{ECL2}A) (data not shown). Interestingly, the cluster of 7 residues at the C-terminal end of the ECL2 that significantly reduced NECA affinity had no impact on NECA efficacy (logτ_c). NECA efficacy was significantly reduced, however, at 5 of the mutant 3xHA-A_1ARs (Fig. 4, Table 1). Of note, NECA efficacy was significantly reduced upon alanine substitution of N148^{ECL2}, E153^{ECL2}, R154^{ECL2} and W156^{ECL2}; mutations that had no significant effect on NECA affinity. In contrast to the effect of L149^{ECL2}A in improving NECA affinity, the same mutation decreased NECA efficacy.

Ligand Docking and Molecular Dynamics Simulations

Molecular Pharmacology Fast Forward. Published on September 28, 2016 as DOI: 10.1124/mol.116.105007
This article has not been copyedited and formatted. The final version may differ from this version.

Inactive and active-like homology models of the human A_1AR were generated based on the antagonist ZM241385 and agonist UK432097 (6-[2,2-di(phenyl)ethylamino]-9-[(2R,3R,4S,5S)-5-(ethylcarbamoyl)-3,4-dihydroxyoxolan-2-yl]-N-[2-[(1-pyridin-2-ylpiperidin-4-yl)carbamoylamino]ethyl]purine-2-carboxamide) occupied crystal structures of the human A_{2A}AR (PDB ID: 3EML and 3QAK), respectively (Jaakola *et al.*, 2008; Xu *et al.*, 2011). Ligand docking and MD simulations were performed using our inactive and active-like A_1AR homology models to assist with the interpretation of mutagenesis findings. The ICM PocketFinder algorithm identified three potential binding pockets within our A_1AR homology models. DPCPX and NECA were docked into the pocket located within the TM bundle, however the size of docking box was adjusted to be large enough to encompass the extracellular region of the receptor. Docking simulations of DPCPX resulted in a single cluster within the TM bundle, where DPCPX formed a π-stacking interaction with $F171^{ECL2}$ (Fig. 5A); this key interaction was maintained during a 40 ns MD simulation (Table 2). Furthermore, the key residue, $N254^{6.55}$, involved in hydrogen bonding interactions in both antagonist and agonist bound A_{2A}AR crystal structures, formed a hydrogen bond with DPCPX during the MD simulation (Table 2). $E172^{ECL2}$, another key residue involved in the formation of the DPCPX binding pocket, that is, found within 3.5 Å of DPCPX during the MD simulation, also decreased [^{3}H]DPCPX affinity when mutated to alanine (Table 2). The root-mean-square-deviation of DPCPX compared to its final pose was calculated. Over the course of the simulation, DPCPX remained relatively stable after 12 ns (Supplemental Fig. 2).

Interestingly, molecular docking of NECA revealed two main clusters amongst the top 40 docking poses, one within the TM bundle ('Site 1') and the other within the extracellular region ('Site 2') (Fig. 5B). Similar findings were also observed when we repeated the molecular docking using the endogenous agonist adenosine instead of NECA (Supplemental Fig 3). The NECA poses found within the TM bundle (Site 1) were located within the predicted A_1AR orthosteric agonist site. Within Site 1, poses could be further divided into two sub-clusters. One sub-cluster had a similar

Molecular Pharmacology Fast Forward. Published on September 28, 2016 as DOI: 10.1124/mol.116.105007
This article has not been copyedited and formatted. The final version may differ from this version.

orientation of the adenine ring to that found within the NECA bound A_{2A}AR crystal structure and was relatively stable during our 40 ns MD simulation (Supplemental Fig. 2). During this simulation, NECA predominantly formed hydrogen bond interactions with the residues T91$^{3.36}$, N254$^{6.55}$ and T277$^{7.42}$. The only ECL2 residue located within 3.5 Å of NECA during this MD simulation was F171^{ECL2} (Table 2). The alternative cluster of NECA Site 1 poses was not considered for MD simulations, as the adenine ring was inverted relative to the position of NECA bound within the A_{2A}AR crystal structure.

NECA poses that docked within the A_1AR extracellular region (Site 2) formed hydrogen bonds with the three extracellular loops and residues at the top of TM6 and TM7. A 40 ns MD simulation was performed on the highest ranked (lowest ICM score) pose within the extracellular vestibule. Within this MD simulation, NECA was relatively stable and formed hydrogen bonds with a number of residues including E170^{ECL2}, E172^{ECL2}, N254$^{6.55}$, K265^{ECL3}, P266^{ECL3} and T270$^{7.35}$ (Table 2; Supplemental Fig. 2). ECL2 residues located within 3.5 Å of NECA during this MD simulation were E170^{ECL2}, F171^{ECL2}, E172^{ECL2} and M177^{ECL2} (Table 2). These findings are consistent with mutagenesis data that suggest each of these residues are involved in the binding of NECA to the A_1AR (Table 1).

A main pose of each ligand, which formed key interactions as determined by the interaction frequency analysis of the MD trajectory, was obtained from each 40 ns MD simulation (Fig. 6, Fig. 7, Data Supplement 1-3). The purine rings for the DPCPX and NECA (Site 1) poses overlap, stabilized by a H-bond with N254$^{6.55}$ and π-stacking interactions with F171^{ECL2} (Supplemental Fig. 4). Residues within the extracellular vestibule, top of TM6 (L250$^{6.51}$, L253$^{6.54}$ and T257$^{6.58}$) and E172^{ECL2} surrounded the DPCPX cyclopentyl ring, whereas the NECA ribose moiety made contacts with residues deeper within the TM bundle (V87$^{3.32}$, L88$^{3.33}$, Q92$^{3.37}$, M180$^{5.40}$, and W247$^{6.48}$). NECA was further anchored by a predicted hydrogen-bond with T91$^{3.36}$ (Fig. 7A, Fig. 7B).

Molecular Pharmacology Fast Forward. Published on September 28, 2016 as DOI: 10.1124/mol.116.105007
This article has not been copyedited and formatted. The final version may differ from this version.

Therefore, the residues predicted to form the NECA Site 1 binding pocket involve conserved residues between the A_1AR and A_{2A}AR, V87$^{3.32}$, L88$^{3.33}$, T91$^{3.36}$, Q92$^{3.37}$, M180$^{5.40}$, W247$^{6.48}$, L250$^{6.51}$ and N254$^{6.55}$. These residues are predicted to be involved in conformational rearrangements of TM3, 5, 6 and 7 upon receptor activation and facilitate the binding of orthosteric agonists (Supplemental Fig. 4)(Xu *et al.*, 2011; Lebon *et al.*, 2011). The main NECA binding pose within Site 2 was predicted to be stabilized by H-bond interactions between the adenine ring and E170^{ECL2}, E172^{ECL2}, S267^{ECL3}, and T270$^{7.35}$ as well as a H-bond between the 2´-OH group of ribose ring and K265^{ECL3} (Fig. 7C, Fig. 7D). The NECA Site 2 binding pocket was also closely packed by F171^{ECL2}, M177^{ECL2} and T257$^{6.58}$ side chains. Interestingly, the NECA (Site 2) and DPCPX poses were not topographically distinct and instead predicted to partially overlap.

Alanine substitution of predicted binding pocket residues from molecular modeling impact NECA affinity and/or efficacy

Results from the NECA Site 1 MD simulations found T91$^{3.36}$, F171^{ECL2} and W247$^{6.48}$ located within 3.5 Å of NECA heavy atoms for at least 60% of the total MD simulation time. Whereas the NECA Site 2 MD simulation found E172^{ECL2}, K265^{ECL3} and T270$^{7.35}$ located within 3.5 Å of NECA heavy atoms for at least 60% of the total MD simulation time. The corresponding conserved residues T91$^{3.36}$, F171^{ECL2} and E172^{ECL2} directly interact with NECA within the A_{2A}AR crystal structure. Furthermore, the involvement of the TM residue T91$^{3.36}$ on A_1AR agonist binding has been confirmed previously through mutagenesis studies (Rivkees *et al.*, 1999). The conserved tryptophan at position 6.48 has been suggested to be involved in the activation process of GPCRs (Shi *et al.*, 2002; Kobilka *et al.*, 2007; Stoddart *et al.*, 2014). Given the known role of T91$^{3.36}$ and W247$^{6.48}$ in A_1AR orthosteric binding, these residues were not investigated further in the current study. However, the influence of the predicted NECA Site 2 residues, K265^{ECL3} and T270$^{7.35}$, on agonist binding or function has not been investigated at the human A_1AR. Therefore, we investigated the influence of single point alanine substitutions of K265^{ECL3}A and T270$^{7.35}$A, on A_1AR

Molecular Pharmacology Fast Forward. Published on September 28, 2016 as DOI: 10.1124/mol.116.105007
This article has not been copyedited and formatted. The final version may differ from this version.

pharmacology. Consistent with DPCPX binding within the TM bundle, neither mutation significantly influenced receptor expression (Fig. 8A) or DPCPX affinity (Fig. 8B). In contrast, alanine substitution of $T270^{7.35}$ caused a significant decrease in NECA affinity (Fig. 8C). Furthermore, both mutations significantly decreased NECA efficacy (Fig. 8D). These data suggest that residues in the extracellular region of the A_1AR play an important role in both agonist binding and function.

Molecular Pharmacology Fast Forward. Published on September 28, 2016 as DOI: 10.1124/mol.116.105007
This article has not been copyedited and formatted. The final version may differ from this version.

Discussion

The A_1AR represents a potential therapeutic target for a number of conditions. A detailed understanding of the structure-function relationships at the A_1AR can facilitate the rational design of more potent and selective A_1AR ligands. Since a high resolution structure of the A_1AR bound to different classes of ligand is not yet available, less direct methods such as site-directed mutagenesis and molecular modeling that can probe the structure-function properties underlying A_1AR orthosteric ligands remain extremely valuable. Given that ECL2 has been suggested to have a critical role in the binding and function of orthosteric ligands at a range of GPCRs (Wheatley *et al.*, 2012), we performed alanine scanning mutagenesis of this region combined with molecular modeling to identify the role of this domain on orthosteric ligand pharmacology. Moreover, key residues predicted from MD to be involved orthosteric agonist function were mutated, and the effects of the mutations validated the importance of these residues. Our A_1AR-ECL2 mutagenesis data are in good agreement with the binding modes of DPCPX and NECA from molecular modeling, identifying a key role for ECL2 in A_1AR orthosteric ligand binding and function. However, our data also suggest that the orthosteric agonist, NECA, recognizes a binding site in an extracellular vestibule that may represent a transition pose prior to entry into the canonical orthosteric site. This vestibular region may represent part of an allosteric binding site for A_1AR modulators, and this is explored in greater detail in our accompanying article.

Previous A_1AR site-directed mutagenesis studies have predominantly focused on TM domains, with residues in TM 1, 2, 3, 4, 5, and 7 implicated in the binding of orthosteric agonists and antagonists (Olah *et al.*, 1994; Townsend-Nicholson and Schofield, 1994; Barbhaiya *et al.*, 1996; Rivkees *et al.*, 1999; Fredholm *et al.*, 2001). Until now, the involvement of ECL2 on orthosteric ligand binding and function has not been systematically investigated at the A_1AR. However, a critical role for this domain on orthosteric pharmacology has been identified from mutagenesis studies on other GPCRs, such as the A_3AR, dopamine D_2 receptor, M_2 and M_3 muscarinic receptors, V_{1a} vasopressin receptor

Molecular Pharmacology Fast Forward. Published on September 28, 2016 as DOI: 10.1124/mol.116.105007
This article has not been copyedited and formatted. The final version may differ from this version.

and glucagon-like peptide-1 receptor (Howl and Wheatley, 1996; Gao *et al.*, 2002; Shi and Javitch, 2004; Duong *et al.*, 2005; Avlani *et al.*, 2007; Scarselli *et al.*, 2007; Koole *et al.*, 2012). It is suggested that orthosteric ligand binding to an unoccupied GPCR, which has a more exposed ECL2, can induce a conformational change, causing ECL2 to close over the entrance to the binding crevice and thereby stabilize the ligand within the orthosteric pocket (Banères *et al.*, 2005; Unal *et al.*, 2010). Supporting this notion, ECL2 contributes to the orthosteric pocket in A_{2A}AR crystal structures. The short helical domain within the A_{2A}AR-ECL2 is oriented towards the TM core region and interacts directly with agonists and antagonists in the orthosteric site (Jaakola *et al.*, 2008; Lebon *et al.*, 2011; Xu *et al.*, 2011; Doré *et al.*, 2011; Congreve *et al.*, 2012; Hino *et al.*, 2012; Liu *et al.*, 2012; Lebon *et al.*, 2015). Molecular modeling performed within the current study, also suggests the short helical domain within the A_1AR-ECL2 forms the upper region of the principal orthosteric pocket. The main pose from MD simulations performed on DPCPX and NECA docked within the TM bundle found two ECL2 residues, F171 and E172, located within 3.5 Å of the orthosteric ligand (Fig. 6, Fig. 7). Supporting a role of these residues in DPCPX binding at the A_1AR, a decrease in [^{3}H]DPCPX and NECA affinity was observed for the E172^{ECL2}A and no [^{3}H]DPCPX binding was observed at the F171^{ECL2}A mutation.

Docking of DPCPX and NECA into homology models based on inactive and active-like A_{2A}AR crystal structures, respectively, revealed overlapping binding poses, with NECA (bound to Site 1) making additional contacts with residues deeper within the TM bundle than DPCPX. Previous studies found that TM3 residues differentially impacted A_1AR orthosteric antagonist versus agonist binding. Mutation of L88$^{3.33}$A caused a substantial reduction of both agonist and antagonist affinity at the A_1AR, whereas and V87$^{3.32}$A has been shown to decrease antagonist affinity alone and Q92$^{3.37}$A has been shown to perturb agonist affinity only (Rivkees *et al.*, 1999). In the main poses after MD simulation, V87$^{3.32}$ and L88$^{3.33}$A were predicted to have hydrophobic interactions with both DPCPX and NECA, while Q92$^{3.37}$ only interacted with NECA (Site 1) (Supplemental Fig. 4).

Molecular Pharmacology Fast Forward. Published on September 28, 2016 as DOI: 10.1124/mol.116.105007
This article has not been copyedited and formatted. The final version may differ from this version.

Therefore, the key interactions predicted from our molecular modelling are in agreement with previous mutagenesis studies and further support a deeper orthosteric-binding pose for NECA (Site 1) relative to the antagonist, DPCPX. It should be noted, however, that the single identified stable pose of the antagonist, DPCPX, is higher-placed such that it overlaps with both NECA-binding clusters i.e., within the orthosteric agonist pocket (Site 1) and the extracellular vestibule (Site 2) to antagonize agonist access.

ECL2 has also been suggested to facilitate ligand access from the extracellular space into the orthosteric TM binding cavity. For instance, in unbiased long time scale MD simulations, β-adrenoceptor orthosteric ligands recognized an intermediate binding site within the extracellular vestibule during the transition from the extracellular space into the TM bundle (Dror *et al.*, 2011). Furthermore, the importance of ECL2 flexibility and conformational integrity was highlighted in a study on the M_2 muscarinic acetylcholine receptor, where a reduction in ECL2 flexibility due to the introduction of a disulfide bond between ECL2 and TM7, caused a significant decrease in orthosteric and allosteric ligand affinity (Avlani *et al.*, 2007). Supporting a role of ECL2 in facilitating ligand entry into the orthosteric site, our docking of NECA in the active-like A_1AR homology model found 31 of the top 40 poses recognized a common site within the extracellular vestibule. The main pose from the MD simulation performed on NECA docked within this site had hydrogen-bonding interactions between the ligand and $E170^{ECL2}$, $E172^{ECL2}$, $K265^{ECL3}$, $S267^{ECL3}$ and $T270^{7.35}$. ECL2 residues located within 3.5 Å of this NECA pose were $E170^{ECL2}$, $F171^{ECL2}$, $E172^{ECL2}$ and $M177^{ECL2}$. Two of these residues, $F171^{ECL2}$ and $E172^{ECL2}$ are also involved in the formation of the orthosteric pocket within the TM bundle. Nonetheless, the existence of the Site 2 binding pocket is supported by ECL2 alanine scanning mutagenesis, which found a significant decrease in NECA affinity at the A_1AR mutations $E170^{ECL2}$A, $E172^{ECL2}$A and $M177^{ECL2}$A. Furthermore, alanine mutation of residues predicted from our MD simulations to interact with NECA at this extracellular site, $K265^{ECL3}$ and $T270^{7.35}$, caused a significant decease in NECA

Molecular Pharmacology Fast Forward. Published on September 28, 2016 as DOI: 10.1124/mol.116.105007
This article has not been copyedited and formatted. The final version may differ from this version.

affinity and/or efficacy. Of note, β_2-adrenoceptor residues that form key interactions with orthosteric ligands within the extracellular vestibule, $Y308^{7.35}$ and $F193^{ECL2}$ (Dror *et al.*, 2011), correspond to $T270^{7.35}$ and $F171^{ECL2}$ identified within our study. Initial recognition within the extracellular vestibule (Site 2) may act as a 'selectivity filter' for GPCRs. The relatively open nature of the extracellular vestibule may lead to Site 2 being more populated by a range of ligands, however only those that form the appropriate metastable poses will eventually transition into Site 1. In contrast, ligands that do not form these metastable interactions within Site 2 will leave this site and dissociate from the receptor. Collectively, these data add weight to the notion that the ECL2 of numerous class A GPCRs contributes to an extracellular vestibule that can bind small molecules, including orthosteric agonists as well as allosteric modulators.

Within this study, alanine mutation of a number of residues in the middle of ECL2, which are predicted from molecular modeling to be distinct from the orthosteric site, caused a significant decrease in orthosteric ligand affinity and/or efficacy. This is perhaps unsurprising given the flexible nature of ECL2 and therefore the spectrum of conformations it likely assumes. Furthermore, ECL2 has not been well defined within A_{2A}AR crystal structures, with many residues not resolved within this region. However, ECL2 residues suggested from alanine scanning mutagenesis to be involved in orthosteric ligand binding may influence the energetics of the unbound receptor conformations and/or facilitate the transition of ligands from the extracellular space into the orthosteric site. Indeed, we identified a cluster of four residues at the TM4 end of ECL2 that perturbed NECA efficacy in the absence of an effect on affinity, indicating that ECL2 is involved in the stabilization of A_1AR active states. These findings are in line with previous studies of other family A GPCRs where mutations within ECL2 perturbed orthosteric agonist efficacy (May *et al.*, 2007; Scarselli *et al.*, 2007; Gregory *et al.*, 2010; 2012; Wifling *et al.*, 2015). At a number of GPCRs, including the M_2 muscarinic acetylcholine and glucagon-like peptide-1 receptor, ECL2 differentially influences orthosteric agonist efficacy depending upon the signalling pathway

Molecular Pharmacology Fast Forward. Published on September 28, 2016 as DOI: 10.1124/mol.116.105007
This article has not been copyedited and formatted. The final version may differ from this version.

assessed (Gregory *et al.*, 2010; 2012; Koole *et al.*, 2012), and as such is thought to play a key role in the stabilization of different active states that contribute to the phenomenon of biased agonism. In the future, it will be pertinent to explore the influence of these ECL2 residues on the bias profile of A_1AR agonists.

Informed by our iterative approach that combined site-directed mutagenesis and molecular modeling with rigorous analysis delineating effects of select A_1AR residues on orthosteric affinity and efficacy, we have demonstrated a key role for ECL2 in A_1AR agonist and antagonist binding and function. Our analysis indicated that agonist ligand affinity and efficacy determinants could be clearly delineated into two major clusters. In addition to making direct contact with ligands bound to the transmembrane bundle, we propose that ECL2 forms an extracellular vestibule that is recognized by, and facilitates the binding of, orthosteric agonists. It would be of interest to determine the extent to which this vestibule also contributes to the actions of A_1AR allosteric ligands.

Molecular Pharmacology Fast Forward. Published on September 28, 2016 as DOI: 10.1124/mol.116.105007
This article has not been copyedited and formatted. The final version may differ from this version.

Acknowledgements

The authors thank Mr Thomas Coudrat for assistance with molecular modeling.

Molecular Pharmacology Fast Forward. Published on September 28, 2016 as DOI: 10.1124/mol.116.105007
This article has not been copyedited and formatted. The final version may differ from this version.

Authorship contributions

Participated in research design: ATNN, LTM, AC

Conducted experiments: ATNN, JB, LLM, KJG

Performed data analysis: ATNN, TDN, TT

Wrote or contributed to the writing of the manuscript: ATNN, PMS, KJG, PJW, LTM, AC

Molecular Pharmacology Fast Forward. Published on September 28, 2016 as DOI: 10.1124/mol.116.105007
This article has not been copyedited and formatted. The final version may differ from this version.

References

Abagyan R, and Kufareva I (2009) The flexible pocketome engine for structural chemogenomics. *Methods Mol Biol* **575**:249–279.

Aksimentiev A, Sotomayor M, and Wells D (2012) Membrane proteins tutorial. http://www.ks.uiuc.edu/Training/Tutorials/science/membrane/mem-tutorial.pdf

An J, Totrov M, and Abagyan R (2005) Pocketome via comprehensive identification and classification of ligand binding envelopes. *Mol Cell Proteomics* **4**:752–761.

Avlani VA, Gregory KJ, Morton CJ, Parker MW, Sexton PM, and Christopoulos A (2007) Critical role for the second extracellular loop in the binding of both orthosteric and allosteric G protein-coupled receptor ligands. *J Biol Chem* **282**:25677–25686.

Ballesteros J, and Weinstein H (1995) Integrated methods for the construction of three dimensional models and computational probing of structure function relations in G-protein-coupled receptors. *Methods Neurosci* **25**:366–428.

Baltos J-A, Gregory KJ, White PJ, Sexton PM, Christopoulos A, and May LT (2016) Quantification of adenosine A_1 receptor biased agonism: Implications for drug discovery. *Biochem Pharmacol* **99**:101–112.

Banères J-L, Mesnier D, Martin A, Joubert L, Dumuis A, and Bockaert J (2005) Molecular characterization of a purified 5-HT4 receptor: a structural basis for drug efficacy. *J Biol Chem* **280**:20253–20260.

Barbhaiya H, McClain R, IJzerman A, and Rivkees SA (1996) Site-directed mutagenesis of the human A_1 adenosine receptor: influences of acidic and hydroxy residues in the first four transmembrane domains on ligand binding. *Mol Pharmacol* **50**:1635–1642.

Black JW, and Leff P (1983) Operational Models of Pharmacological Agonism. *Proc R Soc Lond B Biol Sci* **220**:141–162.

Cheng Y, and Prusoff WH (1973) Relationship between the inhibition constant (K1) and the concentration of inhibitor which causes 50 per cent inhibition (I50) of an enzymatic reaction.

Biochem Pharmacol **22**:3099–3108.

Congreve M, Andrews SP, Doré AS, Hollenstein K, Hurrell E, Langmead CJ, Mason JS, Ng IW, Tehan B, Zhukov A, Weir M, and Marshall FH (2012) Discovery of 1,2,4-Triazine Derivatives as Adenosine A_{2A} Antagonists using Structure Based Drug Design. *J Med Chem* **55**:1898–1903.

Doré AS, Robertson N, Errey JC, Ng I, Hollenstein K, Tehan B, Hurrell E, Bennett K, Congreve M, Magnani F, Tate CG, Weir M, and Marshall FH (2011) Structure of the Adenosine A2A Receptor in Complex with ZM241385 and the Xanthines XAC and Caffeine. *Structure* **19**:1283–1293.

Dror RO, Pan AC, Arlow DH, Borhani DW, Maragakis P, Shan Y, Xu H, and Shaw DE (2011) Pathway and mechanism of drug binding to G-protein-coupled receptors. *Proc Natl Acad Sci USA* **108**:13118–13123.

Duan Y, Wu C, Chowdhury S, Lee MC, Xiong G, Zhang W, Yang R, Cieplak P, Luo R, Lee T, Caldwell J, Wang J, and Kollman P (2003) A point-charge force field for molecular mechanics simulations of proteins based on condensed-phase quantum mechanical calculations. *J Comput Chem* **24**:1999–2012.

Duong HT, Gao Z-G, and Jacobson KA (2005) Nucleoside modification and concerted mutagenesis of the human A_3 adenosine receptor to probe interactions between the 2-position of adenosine analogs and Gln167 in the second extracellular loop. *Nucleosides Nucleotides Nucleic Acids* **24**:1507–1517.

Essmann U, Perera L, Berkowitz ML, Darden T, Lee H, and Pedersen LG (1995) A smooth particle mesh Ewald method. *J Chem Phys* **103**:8577–8593.

Eswar N, Webb B, Marti-Renom MA, Madhusudhan MS, Eramian D, Shen M-Y, Pieper U, and Šali A (2007) Comparative protein structure modeling using MODELLER. *Curr Protoc Protein Sci* **Chapter 2**:Unit 2.9–2.9.31, John Wiley & Sons, Inc.

Fredholm BB, IJzerman AP, Jacobson KA, Klotz K-N, and Linden J (2001) International Union of Pharmacology. XXV. Nomenclature and Classification of Adenosine Receptors. *Pharmacol*

Rev **53**:527–552.

Gao Z-G, Chen A, Barak D, Kim S-K, Müller CE, and Jacobson KA (2002) Identification by Site-directed Mutagenesis of Residues Involved in Ligand Recognition and Activation of the Human A3 Adenosine Receptor. *J Biol Chem* **277**:19056–19063.

Gregory KJ, Hall NE, Tobin AB, Sexton PM, and Christopoulos A (2010) Identification of orthosteric and allosteric site mutations in M_2 muscarinic acetylcholine receptors that contribute to ligand-selective signaling bias. *J Biol Chem* **285**:7459–7474.

Gregory KJ, Sexton PM, Tobin AB, and Christopoulos A (2012) Stimulus bias provides evidence for conformational constraints in the structure of a G protein-coupled receptor. *J Biol Chem* **287**:37066–37077.

Hess S (2001) Recent advances in adenosine receptor antagonist research. *Expert Opin Ther Patents* **11**:1533–1561.

Hino T, Arakawa T, Iwanari H, Yurugi-Kobayashi T, Ikeda-Suno C, Nakada-Nakura Y, Kusano-Arai O, Weyand S, Shimamura T, Nomura N, Cameron AD, Kobayashi T, Hamakubo T, Iwata S, and Murata T (2012) G protein-coupled receptor inactivation by an allosteric inverse-agonist antibody. *Nature* **482**:237–240.

Howl J, and Wheatley M (1996) Molecular recognition of peptide and non-peptide ligands by the extracellular domains of neurohypophysial hormone receptors. *Biochem J* **317 (Pt 2)**:577–582.

Humphrey W, Dalke A, and Schulten K (1996) VMD: visual molecular dynamics. *J Mol Graph* **14**:33–38.

Jaakola V-P, Griffith MT, Hanson MA, Cherezov V, Chien EYT, Lane JR, IJzerman AP, and Stevens RC (2008) The 2.6 Angstrom Crystal Structure of a Human A_{2A} Adenosine Receptor Bound to an Antagonist. *Science* **322**:1211–1217.

Jacobson KA, and Gao Z-G (2006) Adenosine receptors as therapeutic targets. *Nat Rev Drug Discov* **5**:247–264.

Kalk P, Eggert B, Relle K, Godes M, Heiden S, Sharkovska Y, Fisher Y, Zeigler D, Bielenberg G-

W, Hocher B (2007) The adenosine A_1 receptor antagonist SLV320 reduces myocardial fibrosis in rats with 5/6 nephrectomy without affecting blood pressure. *Br J Pharmacol* **151**:1025-1032

Kim J, Jiang Q, Glashofer M, Yehle S, Wess J, and Jacobson KA (1996) Glutamate residues in the second extracellular loop of the human A_{2A} adenosine receptor are required for ligand recognition. *Mol Pharmacol* **49**:683–691.

Kobilka BK (2007) G protein coupled receptor structure and activation. *Biochim Biophys Acta* **1768**:794-807.

Koole C, Wootten D, Simms J, Miller LJ, Christopoulos A, and Sexton PM (2012) Second Extracellular Loop of Human Glucagon-like Peptide-1 Receptor (GLP-1R) has a Critical Role in GLP-1 Peptide Binding and Receptor Activation. *J Biol Chem* **287**:3642–3658.

Leach K, Davey AE, Felder CC, Sexton PM, and Christopoulos A (2011) The Role of Transmembrane Domain 3 in the Actions of Orthosteric, Allosteric, and Atypical Agonists of the M4 Muscarinic Acetylcholine Receptor. *Mol Pharmacol* **79**:855–865.

Lebon G, Edwards PC, Leslie AGW, and Tate CG (2015) Molecular Determinants of CGS21680 Binding to the Human Adenosine A_{2A} Receptor. *Mol Pharmacol* **87**:907–915.

Lebon G, Warne T, Edwards PC, Bennett K, Langmead CJ, Leslie AGW, and Tate CG (2011) Agonist-bound adenosine A_{2A} receptor structures reveal common features of GPCR activation. *Nature* **474**:521–525.

Liu W, Chun E, Thompson AA, Chubukov P, Xu F, Katritch V, Han GW, Roth CB, Heitman LH, IJzerman AP, Cherezov V, and Stevens RC (2012) Structural Basis for Allosteric Regulation of GPCRs by Sodium Ions. *Science* **337**:232–236.

Mackerell AD Jr., Feig M, and Brooks CL III (2004) Extending the treatment of backbone energetics in protein force fields: Limitations of gas-phase quantum mechanics in reproducing protein conformational distributions in molecular dynamics simulations. *J Comput Chem* **25**:1400–1415.

MacKerell AD, Bashford D, Bellott, Dunbrack RL, Evanseck JD, Field MJ, Fischer S, Gao J, Guo

H, Ha S, Joseph-McCarthy D, Kuchnir L, Kuczera K, Lau FTK, Mattos C, Michnick S, Ngo T, Nguyen DT, Prodhom B, Reiher WE, Roux B, Schlenkrich M, Smith JC, Stote R, Straub J, Watanabe M, Wiórkiewicz-Kuczera J, Yin D, and Karplus M (1998) All-Atom Empirical Potential for Molecular Modeling and Dynamics Studies of Proteins. *J Phys Chem B* **102**:3586–3616.

Martinelli A, and Tuccinardi T (2008) Molecular modeling of adenosine receptors: new results and trends. *Med Res Rev* **28**:247–277.

May LT, Avlani VA, Langmead CJ, Herdon HJ, Wood MD, Sexton PM, and Christopoulos A (2007) Structure-Function Studies of Allosteric Agonism at M_2 Muscarinic Acetylcholine Receptors. *Mol Pharmacol* **72**:463–476.

Müller CE, and Jacobson KA (2011) Recent developments in adenosine receptor ligands and their potential as novel drugs. *BBA - Biomembranes* **1808**:1290–1308

Olah ME, Jacobson KA, and Stiles GL (1994) Role of the second extracellular loop of adenosine receptors in agonist and antagonist binding. Analysis of chimeric A_1/A_3 adenosine receptors. *J Biol Chem* **269**:24692–24698.

Palmer TM, and Stiles GL (1995) Adenosine receptors. *Neuropharmacology* **34**:683–694.

Phillips JC, Braun R, Wang W, Gumbart J, Tajkhorshid E, Villa E, Chipot C, Skeel RD, Kalé L, and Schulten K (2005) Scalable molecular dynamics with NAMD. *J Comput Chem* **26**:1781–1802.

Rivkees SA, Barbhaiya H, and IJzerman AP (1999) Identification of the adenine binding site of the human A_1 adenosine receptor. *J Biol Chem* **274**:3617–3621.

Sabbadin D, Ciancetta A, Deganutti G, Cuzzolin A, Moro S (2015) Exploring the recognition pathway at the human A_{2A} adenosine receptor of the endogenous agonist adenosine using supervised molecular dynamics. *Med. Chem. Commun.* **6**:1081-1085.

Scarselli M, Li B, Kim S-K, and Wess J (2007) Multiple residues in the second extracellular loop are critical for M_3 muscarinic acetylcholine receptor activation. *J Biol Chem* **282**:7385–7396.

Schiedel AC, Hinz S, Thimm D, Sherbiny F, Borrmann T, Maaß A, and Müller CE (2011) The four cysteine residues in the second extracellular loop of the human adenosine A_{2B} receptor: Role in ligand binding and receptor function. *Biochem Pharmacol* **82**:389–399.

Scholl DJ, and Wells JN (2000) Serine and alanine mutagenesis of the nine native cysteine residues of the human A(1) adenosine receptor. *Biochem Pharmacol* **60**:1647–1654.

Shi L, and Javitch JA (2004) The second extracellular loop of the dopamine D_2 receptor lines the binding-site crevice. *Proc Natl Acad Sci USA* **101**:440–445.

Shi L, Liapakis G, Xu R, Guarnieri F, Ballesteros J, and Javitch JA (2002) Beta2 adrenergic receptor activation. Modulation of the proline kink in transmembrane 6 by a rotamer toggle switch. *J Biol Chem* **277**:40989–40996.

Shonberg J, Klein Herenbrink C, Lopez Munoz L, Christopoulos A, Scammells PJ, Capuano B, and Lane JR (2013) A Structure-Activity Analysis of Biased Agonism at the Dopamine D2 Receptor. *J Med Chem* **56**:9199-9221.

Sromek SM, and Harden TK (1998) Agonist-induced internalization of the P2Y2 receptor. *Mol Pharmacol* **54**:485–494.

Stoddart LA, Kellam B, Briddon SJ, and Hill SJ (2014) Effect of a toggle switch mutation in TM6 of the human adenosine A_3 receptor on Gi protein-dependent signalling and Gi-independent receptor internalization. *Br J Pharmacol* **171**:3827-3844

Thompson JD, Gibson TJ, Plewniak F, Jeanmougin F, and Higgins DG (1997) The CLUSTAL_X windows interface: flexible strategies for multiple sequence alignment aided by quality analysis tools. *Nucleic Acids Res* **25**:4876–4882.

Townsend-Nicholson A, and Schofield PR (1994) A threonine residue in the seventh transmembrane domain of the human A1 adenosine receptor mediates specific agonist binding. *J Biol Chem* **269**:2373–2376.

Unal H, Jagannathan R, Bhat MB, and Karnik SS (2010) Ligand-specific conformation of extracellular loop-2 in the angiotensin II type 1 receptor. *J Biol Chem* **285**:16341–16350.

Valant C, May LT, Aurelio L, Chuo CH, White PJ, Baltos J-A, Sexton PM, Scammells PJ, and Christopoulos A (2014) Separation of on-target efficacy from adverse effects through rational design of a bitopic adenosine receptor agonist. *Proc Natl Acad Sci USA* **111**:4614–4619.

Vanommeslaeghe K, Hatcher E, Acharya C, Kundu S, Zhong S, Shim J, Darian E, Guvench O, Lopes P, Vorobyov I, and MacKerell AD (2010) CHARMM general force field: A force field for drug-like molecules compatible with the CHARMM all-atom additive biological force fields. *J Comput Chem* **31**:671–690.

Vecchio EA, Tan CY, Gregory KJ, Christopoulos A, White PJ, and May LT (2016) Ligand-independent adenosine A2B receptor constitutive activity as a promoter of prostate cancer cell proliferation. *J Pharmacol Exp Ther* **357:**36-44.

Wheatley M, Wootten D, Conner MT, Simms J, Kendrick R, Logan RT, Poyner DR, and Barwell J (2012) Lifting the lid on GPCRs: the role of extracellular loops. *Br J Pharmacol* **165**:1688–1703.

Wifling D, Bernhardt G, Dove S, and Buschauer A (2015) The Extracellular Loop 2 (ECL2) of the Human Histamine H 4 Receptor Substantially Contributes to Ligand Binding and Constitutive Activity. *PLoS One* **10**:e0117185.

Xu F, Wu H, Katritch V, Han GW, Jacobson KA, Gao ZG, Cherezov V, and Stevens RC (2011) Structure of an Agonist-Bound Human A2A Adenosine Receptor. *Science* **332**:322–327.

Yaar R, Jones MR, Chen J-F, and Ravid K (2004) Animal models for the study of adenosine receptor function. *J Cell Physiol* **202**:9–20.

Yu W, He X, Vanommeslaeghe K, and MacKerell AD (2012) Extension of the CHARMM General Force Field to sulfonyl-containing compounds and its utility in biomolecular simulations. *J Comput Chem* **33**:2451–2468.

Molecular Pharmacology Fast Forward. Published on September 28, 2016 as DOI: 10.1124/mol.116.105007
This article has not been copyedited and formatted. The final version may differ from this version.

Footnotes

This work was funded by the National Health and Medical Research Council of Australia (NHMRC) [Program Grant APP1055134, Project Grant APP1084487, Project Grant APP1084246]. ATNN is a recipient of an Australian Endeavour Scholarship and Fellowship. LTM is a recipient of an Australian Research Council (ARC) Discovery Early Career Researcher Award (DECRA), AC is a Senior Principal Research Fellow, and PMS is a Principal Research Fellow, of the NHMRC. KJG is a NHMRC Overseas Biomedical Postdoctoral Training Fellow.

Molecular Pharmacology Fast Forward. Published on September 28, 2016 as DOI: 10.1124/mol.116.105007
This article has not been copyedited and formatted. The final version may differ from this version.

FIGURE LEGENDS

Fig. 1. A) Diagram highlighting alanine mutations within the human A_1AR. Single alanine substitutions are highlighted in red whereas double and triple mutations are blue. **B**) Receptor expression (B_{max}) of WT and mutant 3xHA-A_1ARs stably expressed in Flp-In™-CHO cells. B_{max} values are expressed as a percentage of WT and represent the mean ± S.E.M of at least 3 experiments performed in duplicate. *P < 0.05 compared to WT (one-way analysis of variance, Dunnett's post hoc test). ND, not determined as no specific radioligand binding detected.

Fig. 2. Radioligand binding and cAMP accumulation data for Flp-In™-CHO cells stably expressing WT or selected mutant 3xHA-A_1ARs. **A**) [^{3}H]DPCPX whole cell saturation binding, **B**) [^{3}H]DPCPX whole cell competition binding and **C**) cAMP accumulation. Data are mean ± S.E.M from at least 3 experiments conducted in duplicate. Where error bars are not shown they lie within the dimensions of the symbol.

Fig. 3. The change in affinity of **A)** DPCPX (ΔpK_D) and **B)** NECA (ΔpK_I) at mutant 3xHA-A_1ARs relative to WT. Data represents the mean ± S.E.M of at least 3 experiments performed in duplicate. *P < 0.05 compared to WT (one-way analysis of variance, Dunnett's post hoc test).

Fig. 4. The change in signaling efficacy of NECA ($\Delta \log \tau_c$) at mutant 3xHA-A_1ARs relative to WT. Data represent the mean ± S.E.M of at least 3 experiments performed in duplicate. *P < 0.05 compared to WT (one-way analysis of variance, Dunnett's post hoc test).

Fig. 5. Docking of DPCPX and NECA into A_1AR homology models. **A)** The top 20 DPCPX (sticks; carbon, nitrogen, oxygen and polar hydrogen atoms are colored in cyan, blue, red and white, respectively) poses docked into the inactive A_1AR homology model (grey ribbons). $F171^{ECL2}$,

Molecular Pharmacology Fast Forward. Published on September 28, 2016 as DOI: 10.1124/mol.116.105007
This article has not been copyedited and formatted. The final version may differ from this version.

predicted to form a key π-stacking interaction with DPCPX, is shown as blue sticks. **B)** The top 40 NECA (sticks; carbon, nitrogen, oxygen and polar hydrogen atoms are colored in green, blue, red and white, respectively) poses docked into the active-like A_1AR homology model (light blue ribbons). Residues predicted to be involved in hydrogen bond and π-stacking interactions are shown as blue sticks.

Fig. 6. Predicted binding mode of DPCPX (cyan sticks) at the inactive A_1AR homology model (grey ribbons). Residues that significantly influenced DPCPX affinity are shown as yellow (<5 fold change) and orange (between 5-10 fold change) sticks. Key residues predicted to form hydrogen bond ($N254^{6.55}$) or π-stacking ($F171^{ECL2}$) interactions with DPCPX are shown as blue sticks.

Fig. 7. Predicted binding mode of NECA (green sticks) at the partially active A_1AR homology model (light blue ribbons) located in the orthosteric site (Site 1; **A** and **B**) and extracellular vestibule (Site 2; **C** and **D**). Residues that significantly influenced NECA affinity (**A**, **C**) or efficacy (**B**, **D**) are shown as yellow (<5 fold change), orange (between 5-10 fold change) and red (>10 fold change) sticks. Key residues predicted to form hydrogen bond interactions with NECA are shown as blue sticks.

Fig. 8. The influence of alanine substitution on residues predicted from MD simulations to be involved Site 2 NECA binding. **A**) Receptor expression (B_{max}) of WT and mutant 3xHA-A_1ARs stably expressed in Flp-In™-CHO cells. B_{max} values are expressed as a percentage of WT. The change in [^{3}H]DPCPX affinity (**B**), NECA affinity (**C**) and NECA efficacy (**D**) for mutant 3xHA-A_1ARs relative to WT. Data represents the mean ± S.E.M of 3 experiments performed in duplicate. *P < 0.05 compared to WT (one-way analysis of variance, Dunnett's post hoc test).

Molecular Pharmacology Fast Forward. Published on September 28, 2016 as DOI: 10.1124/mol.116.105007
This article has not been copyedited and formatted. The final version may differ from this version.

Table 1. Orthosteric whole cell equilibrium binding and agonist operational efficacy parameters at WT and mutant A_1ARs mutant 3xHA-A_1ARs stably expressed in Flp-In™-CHO cells. pK_D and pK_I are the negative logarithm of the radioligand [^{3}H]DPCPX and NECA equilibrium dissociation constants, respectively. Logτ_c is logarithm of operational efficacy parameter for NECA determined using operational model of agonism, where NECA pK_I values were constrained to those determined from the radioligand binding assays. Values represent the mean ± S.E.M. from the indicated number of individual experiments (n) performed in in duplicate.

	[^{3}H]DPCPX	NECA	
	pK_D (n)	pK_I (n)	logτ_c[a] (n)
WT	9.17 ± 0.04 (16)	6.59 ± 0.04 (44)	1.78 ± 0.09 (20)
F144A	9.23 ± 0.06 (5)	6.62 ± 0.13 (10)	1.58 ± 0.05 (6)
G145A	9.00 ± 0.02 (5)	6.38 ± 0.08 (9)	1.46 ± 0.02 (6)
W146A	8.97 ± 0.12 (5)	6.20 ± 0.17 (6)*	1.63 ± 0.06 (6)
N147A	9.08 ± 0.09 (5)	6.40 ± 0.14 (6)	1.63 ± 0.06 (5)
N148A	8.98 ± 0.08 (4)	6.70 ± 0.09 (8)	1.21 ± 0.09 (4)*
L149A	9.35 ± 0.10 (6)	6.94 ± 0.10 (8)*	0.86 ± 0.35 (3)*
SV150AA	8.81 ± 0.14 (3)	6.37 ± 0.13 (10)	2.15 ± 0.31 (3)
E153A	9.17 ± 0.09 (5)	6.58 ± 0.07 (11)	1.34 ± 0.04 (6)*
R154A	9.06 ± 0.07 (5)	6.52 ± 0.07 (13)	1.16 ± 0.22 (5)*
W156A	9.07 ± 0.07 (5)	6.5 ± 0.09 (12)	0.89 ± 0.19 (6)*
N159A	8.56 ± 0.11 (9)*	5.95 ± 0.06 (12)*	1.64 ± 0.08 (6)
G160A	9.30 ± 0.12 (5)	6.80 ± 0.10 (10)	1.46 ± 0.12 (5)
S161A	8.66 ± 0.13 (6)*	6.10 ± 0.10 (8)*	1.73 ± 0.09 (5)
MGE162AAA	8.82 ± 0.08 (3)	6.43 ± 0.08 (9)	2.17 ± 0.23 (3)

Molecular Pharmacology Fast Forward. Published on September 28, 2016 as DOI: 10.1124/mol.116.105007
This article has not been copyedited and formatted. The final version may differ from this version.

P165A	9.05 ± 0.08 (3)	6.45 ± 0.08 (10)	1.72 ± 0.05 (7)
V166A	9.05 ± 0.11 (3)	6.45 ± 0.10 (12)	1.72 ± 0.06 (7)
I167A	8.42 ± 0.13 (6) *	5.74 ± 0.06 (12)*	1.45 ± 0.04 (7)
K168A	9.12 ± 0.06 (3)	6.43 ± 0.04 (12)	1.69 ± 0.09 (7)
E170A	9.24 ± 0.15 (3)	6.22 ± 0.06 (12)*	1.56 ± 0.05 (7)
F171A	NA	NA	NA
E172A	8.66 ± 0.20 (3)*	5.84 ± 0.08 (11)*	1.57 ± 0.14 (9)
K173A	9.21 ± 0.02 (3)	6.42 ± 0.08 (11)	1.56 ± 0.05 (7)
V174A	9.12 ± 0.13 (3)	6.46 ± 0.10 (8)	1.50 ± 0.03 (7)
I175A	8.45 ± 0.10 (5)*	5.56 ± 0.08 (7)*	1.45 ± 0.06 (5)
S176A	9.08 ± 0.14 (3)	6.38 ± 0.06 (13)	1.54 ± 0.03 (7)
M177A	8.39 ± 0.17 (6)*	5.81 ± 0.05 (11)*	1.52 ± 0.05 (7)
K265A (ECL3)	8.98 ± 0.09 (4)	6.34 ± 0.04 (6)	1.18 ± 0.15 (6)*
T270A (7.35)	8.83 ± 0.04 (3)	5.76 ± 0.05* (13)	1.48 ± 0.06 (12)*

[a] $Log\tau_c$ values are corrected for changes in receptor expression by fold-normalization to the B_{max} value of the WT receptor. A transducer slope of 1.17 was shared across all data sets, as the fit was not significantly improved by allowing separate transducer slope values for the different constructs (as determined by an Extra-sum-of-squares, F test).

*Significantly different from WT value ($p < 0.05$, one-way ANOVA with Dunnet's post-hoc test)

NA, not applicable (no competition with the radioligand or no inhibition of cAMP)

Molecular Pharmacology Fast Forward. Published on September 28, 2016 as DOI: 10.1124/mol.116.105007
This article has not been copyedited and formatted. The final version may differ from this version.

Table 2. A_1AR residues that interact with DPCPX or NECA through the course of each MD simulations. Values represent the percentage of the MD simulation time (40 ns) that the residue and ligand heavy atoms are within 3.5 Å of one another. Residues were considered to be interacting with the ligand if they were in contact with the ligand for >5% of simulation time. Hydrogen-bond interactions (in bracket) were defined with the donor- acceptor distance < 3.5 Å, and an angle cutoff of 20° and displayed as percentage of MD simulation time. All values were calculated for 1 frame per 10 ps using VMD v1.9.2.

Residues	**DPCPX**	**NECA Site 1**	**NECA Site 2**
$V62^{2.56}$	-	5.7	-
$I69^{2.63}$	14.1	-	-
$N70^{ECL1}$	8.9	-	5.4
$V87^{3.32}$	54.0	26.6	-
$L88^{3.33}$	-	20.3	-
$T91^{3.36}$	14.7	99.6 (L-RS: 44.4)	-
$Q92^{3.37}$	-	22.3	-
$E170^{ECL2}$	-	-	46 (L-RS: 19.7)
$F171^{ECL2}$	81.5	65.9	11.4
$E172^{ECL2}$	6.9	16.5	64.8
$M177^{ECL2}$	-	-	25.6
$M180^{5.40}$	38.7	40.3	-
$N184^{5.43}$	-	37.9	-
$W247^{6.48}$	34.2	63.9	-
$L250^{6.51}$	22.9	9.0	-

Molecular Pharmacology Fast Forward. Published on September 28, 2016 as DOI: 10.1124/mol.116.105007
This article has not been copyedited and formatted. The final version may differ from this version.

H251$^{6.52}$	-	9.1	-
L253$^{6.54}$	8.9	-	-
N254$^{6.55}$	90.8 (L-RS: 38.7 RS-L: 14.4)	57.6 (L-RS: 12.9 RS-L: 10.2)	27.8
T257$^{6.58}$	51.8	-	15.1
H264^{ECL3}	-	-	32.4
K265^{ECL3}	-	-	98.1 (L-RM: 39.4 RM-L: 13.2)
P266^{ECL3}	-	-	98.1
S267^{ECL3}	-	-	57.5
T270$^{7.35}$	6.8	-	76.4 (L-RS: 5.8 RS-L: 14.1)
Y271$^{7.36}$	-	-	44.9
I274$^{7.39}$	18.6	29.8	-
T277$^{7.42}$	-	42.9 (L-RS: 1.2 RS-L:4.5)	-
H278$^{7.43}$	-	12.1	-

L-RS: hydrogen-bond interaction between ligand (donor) and residue side chain (acceptor)

RS-L: hydrogen-bond interaction between residue side chain (donor) and ligand (acceptor)

L-RM: hydrogen-bond interaction between ligand (donor) and residue main chain (acceptor)

RM-L: hydrogen-bond interaction between residue main chain (donor) and ligand (acceptor)

Fig. 1

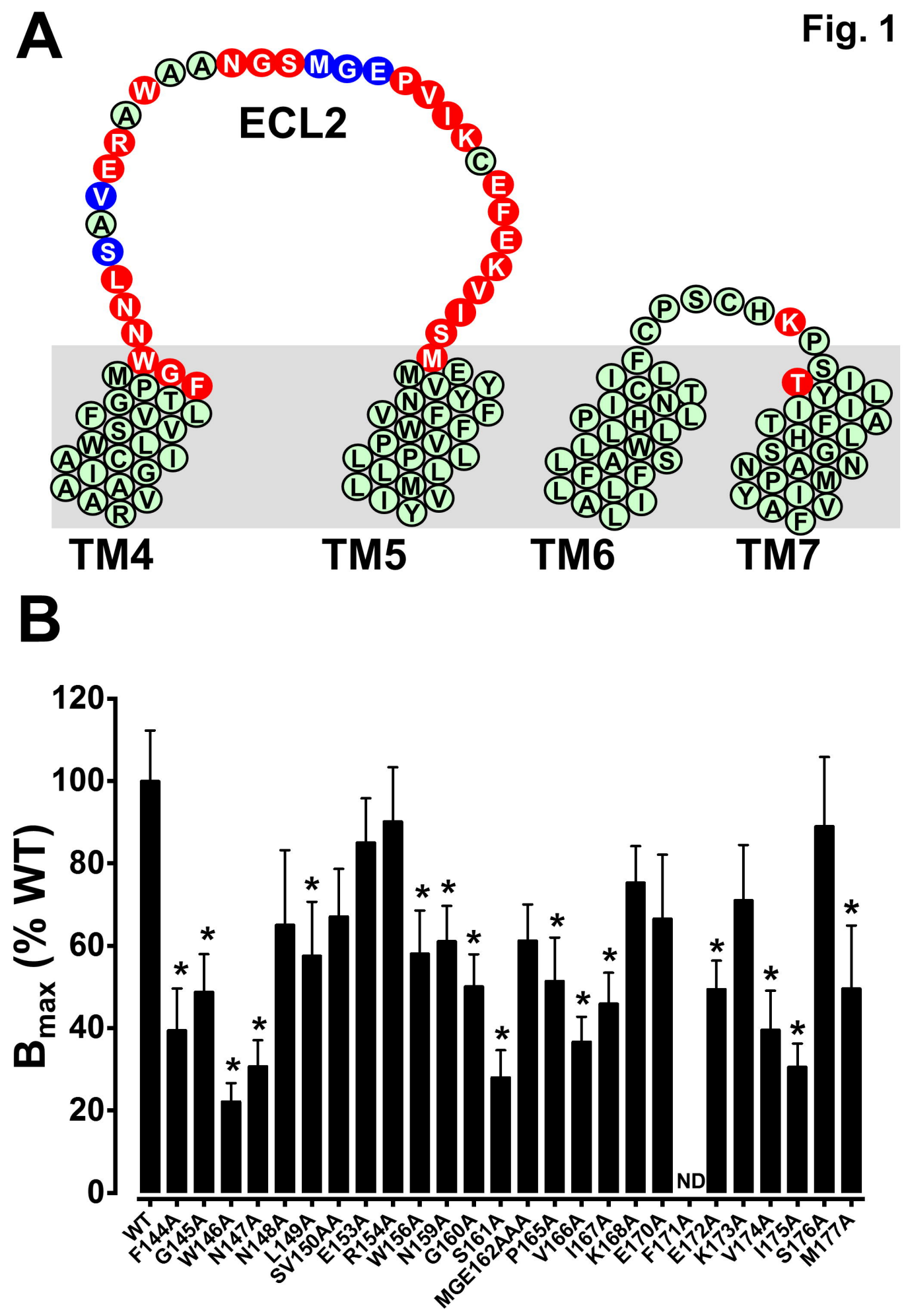
A
ECL2
TM4
TM5
TM6
TM7
B
B_{max} (% WT)
120
100
80
60
40
20
0
ND
WT
F144A
G145A
W146A
N147A
N148A
L149A
SV150AA
E153A
R154A
W156A
N159A
G160A
S161A
MGE162AAA
P165A
V166A
I167A
K168A
E170A
F171A
E172A
K173A
V174A
I175A
S176A
M177A

Fig. 2

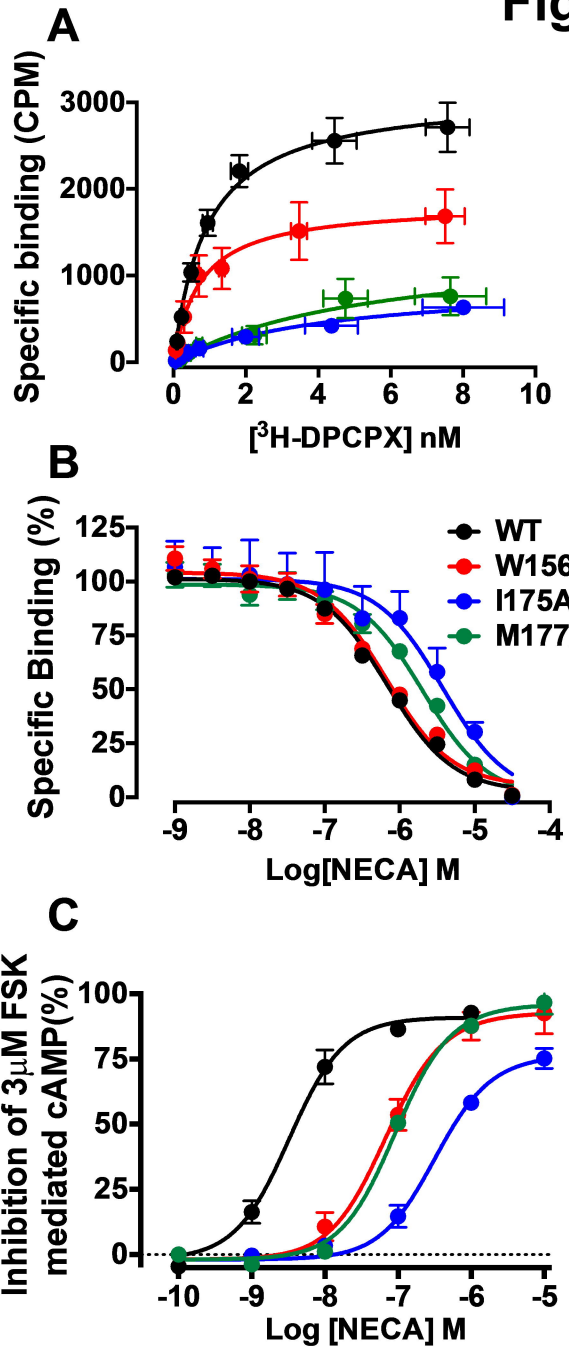
A
Specific binding (CPM)
3000
2000
1000
0
0
2
4
6
8
10
[3H-DPCPX] nM
B
Specific Binding (%)
125
100
75
50
25
0
WT
W156A
I175A
M177A
-9
-8
-7
-6
-5
-4
Log[NECA] M
C
Inhibition of 3μM FSK mediated cAMP(%)
100
75
50
25
0
-10
-9
-8
-7
-6
-5
Log [NECA] M

Fig. 3

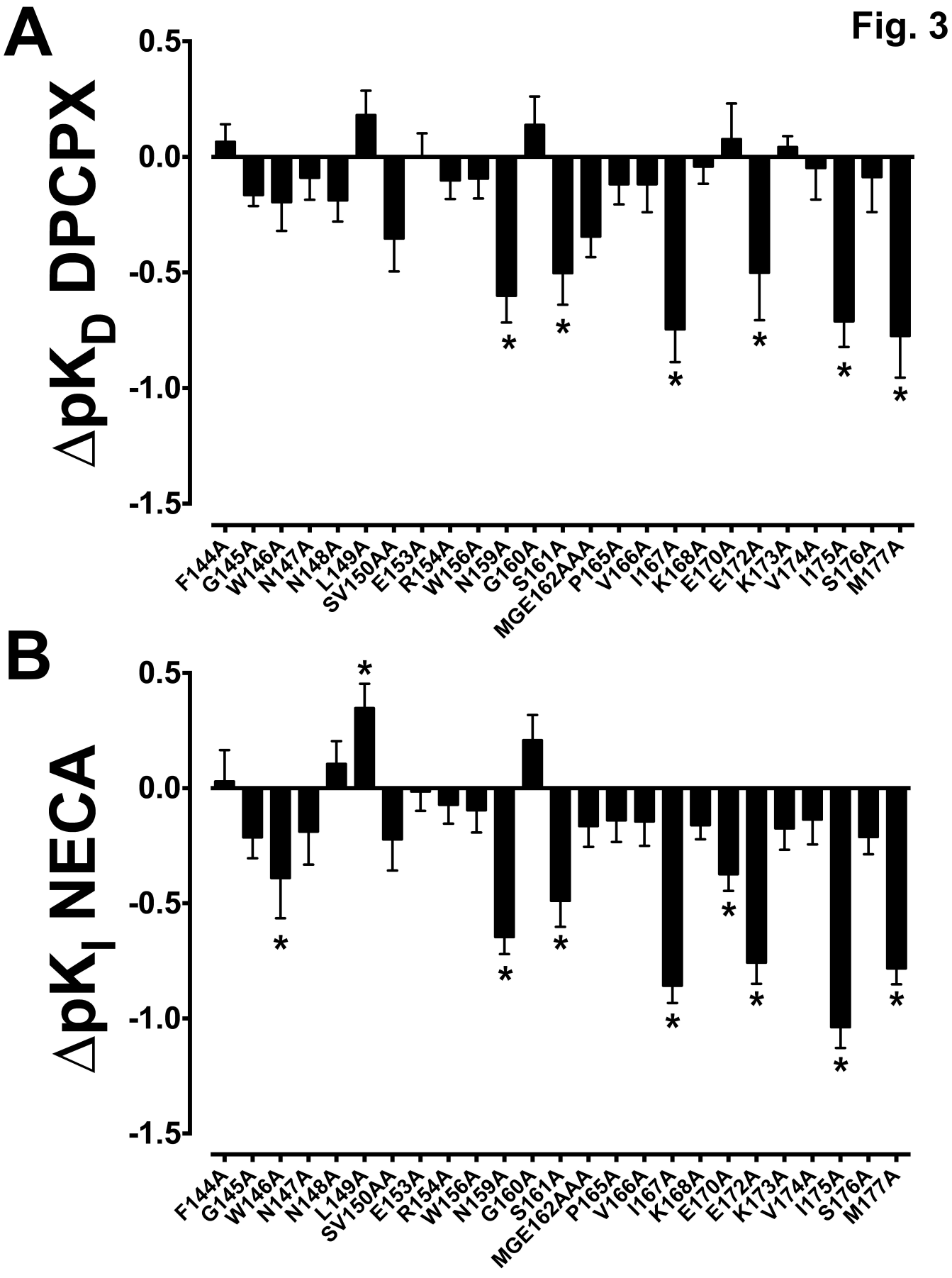
A
ΔpK_D DPCPX
0.5
0.0
-0.5
-1.0
-1.5
F144A
G145A
W146A
N147A
N148A
L149A
SV150AA
E153A
R154A
W156A
N159A
G160A
S161A
MGE162AAA
P165A
V166A
I167A
K168A
E170A
E172A
K173A
V174A
I175A
S176A
M177A
B
ΔpK_I NECA
0.5
0.0
-0.5
-1.0
-1.5
F144A
G145A
W146A
N147A
N148A
L149A
SV150AA
E153A
R154A
W156A
N159A
G160A
S161A
MGE162AAA
P165A
V166A
I167A
K168A
E170A
E172A
K173A
V174A
I175A
S176A
M177A

Fig. 4

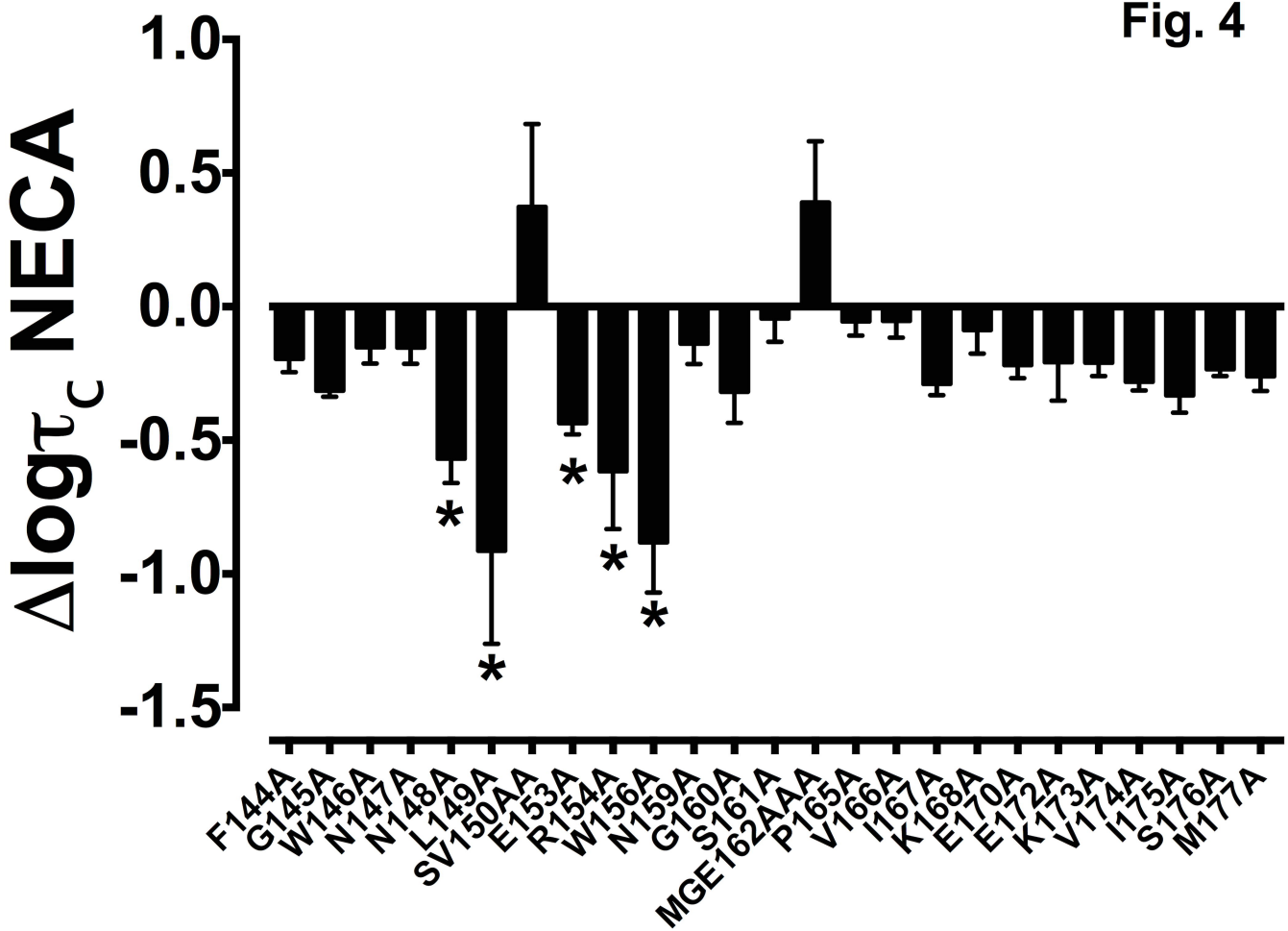
1.0
0.5
0.0
-0.5
-1.0
-1.5
Δlogτc NECA
*
*
*
*
*
F144A
G145A
W146A
N147A
N148A
L149A
SV150AA
E153A
R154A
W156A
N159A
G160A
S161A
MGE162AAA
P165A
V166A
I167A
K168A
E170A
E172A
K173A
V174A
I175A
S176A
M177A

Fig. 5

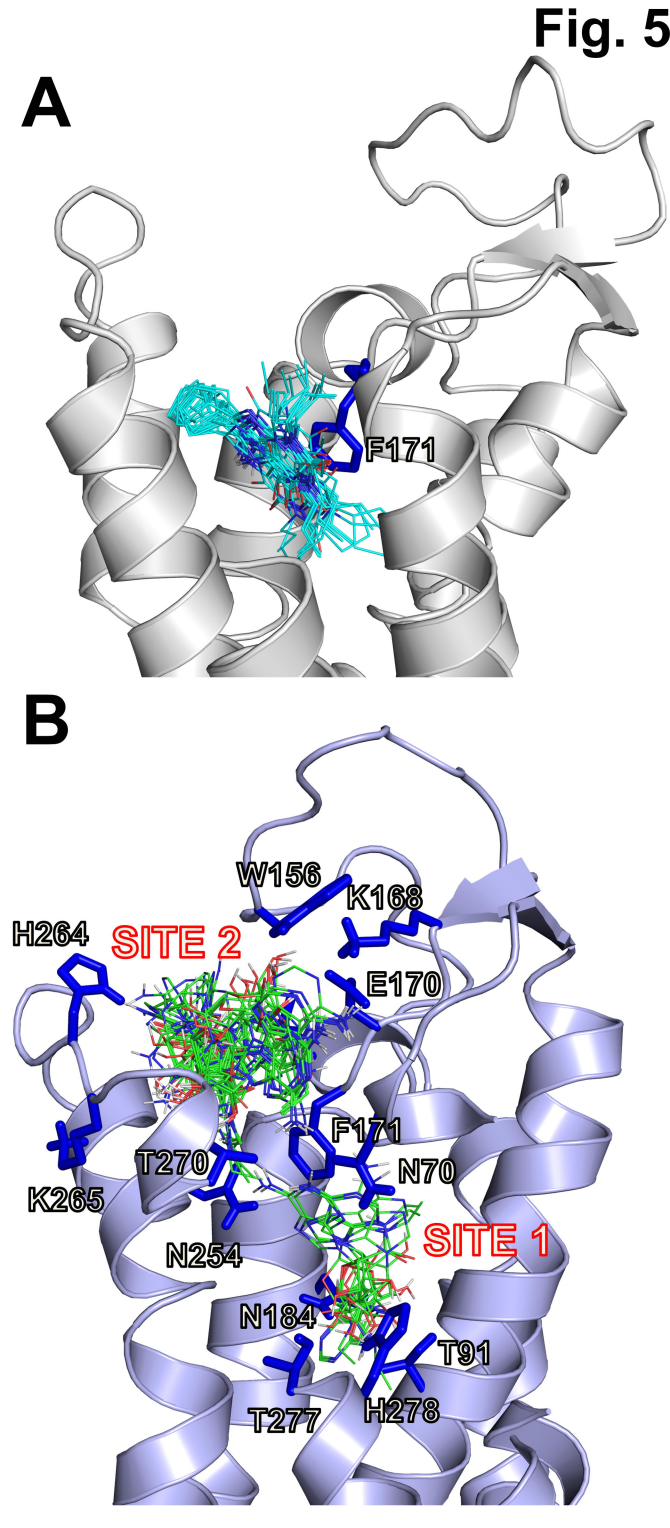
A
F171
B
W156
K168
H264
SITE 2
E170
F171
T270
N70
K265
SITE 1
N254
N184
T91
T277
H278

Fig. 6

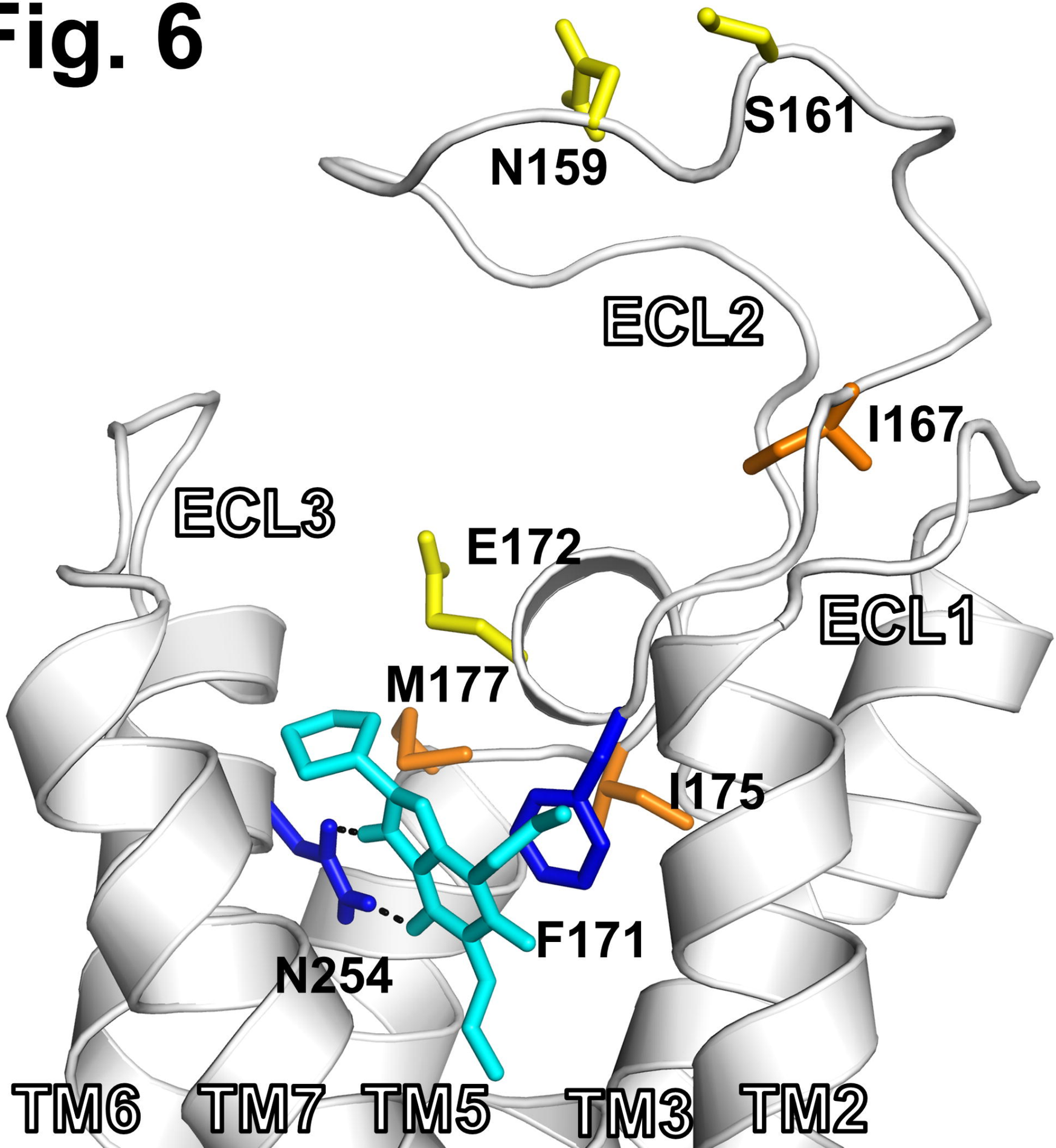
S161
N159
ECL2
I167
ECL3
E172
ECL1
M177
I175
F171
N254
TM6
TM7
TM5
TM3
TM2

Fig. 7

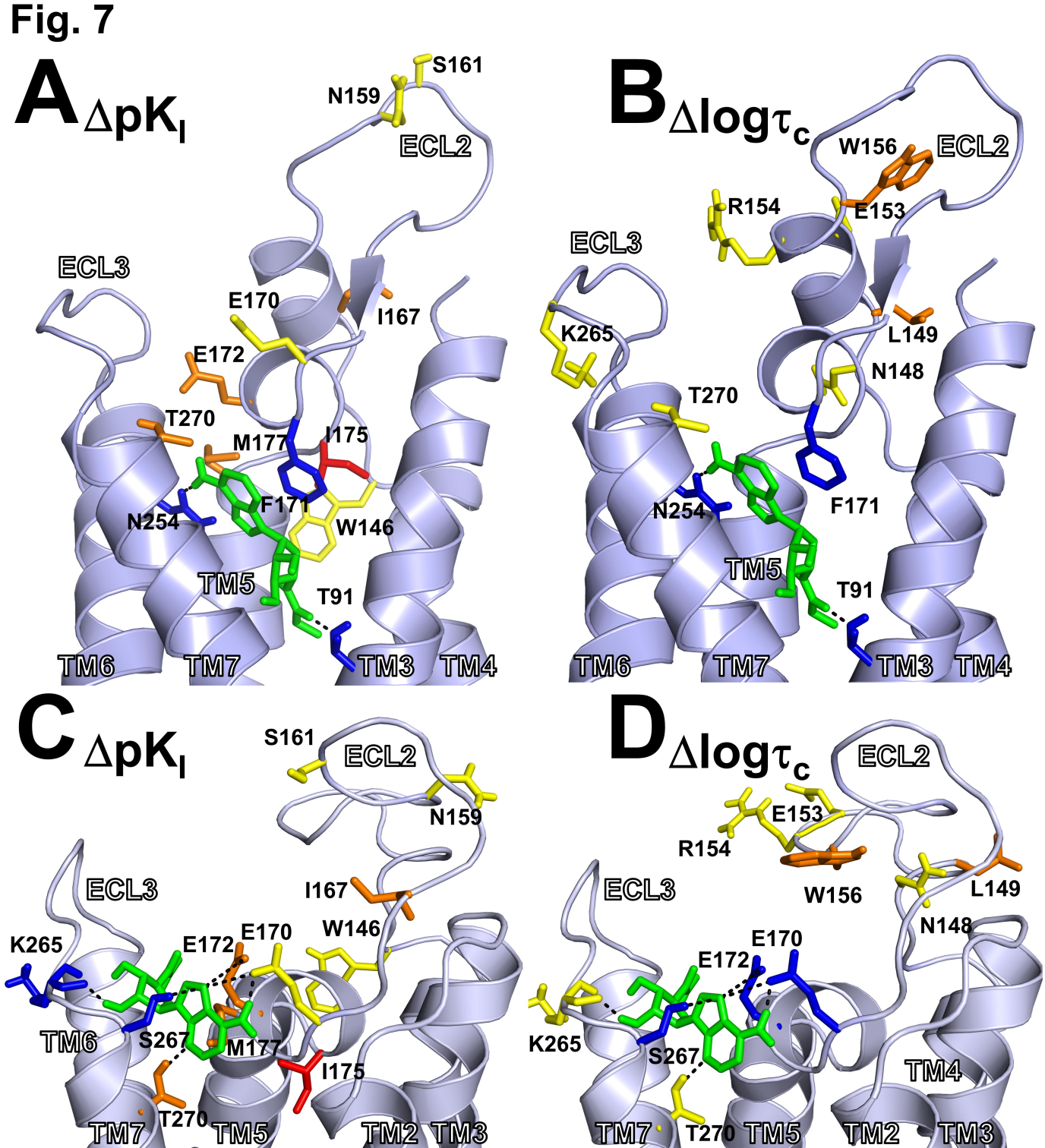
A ΔpK_I
S161
N159
ECL2
ECL3
E170
I167
E172
T270
M177
I175
F171
N254
W146
TM5
T91
TM6
TM7
TM3
TM4
B Δlogτ_c
W156
ECL2
R154
E153
ECL3
K265
L149
N148
T270
N254
F171
TM5
T91
TM6
TM7
TM3
TM4
C ΔpK_I
S161
ECL2
N159
ECL3
I167
K265
E172
E170
W146
TM6
S267
M177
I175
T270
TM7
TM5
TM2
TM3
D Δlogτ_c
ECL2
E153
R154
ECL3
W156
L149
N148
E170
E172
K265
S267
TM4
TM7
T270
TM5
TM2
TM3

Fig. 8

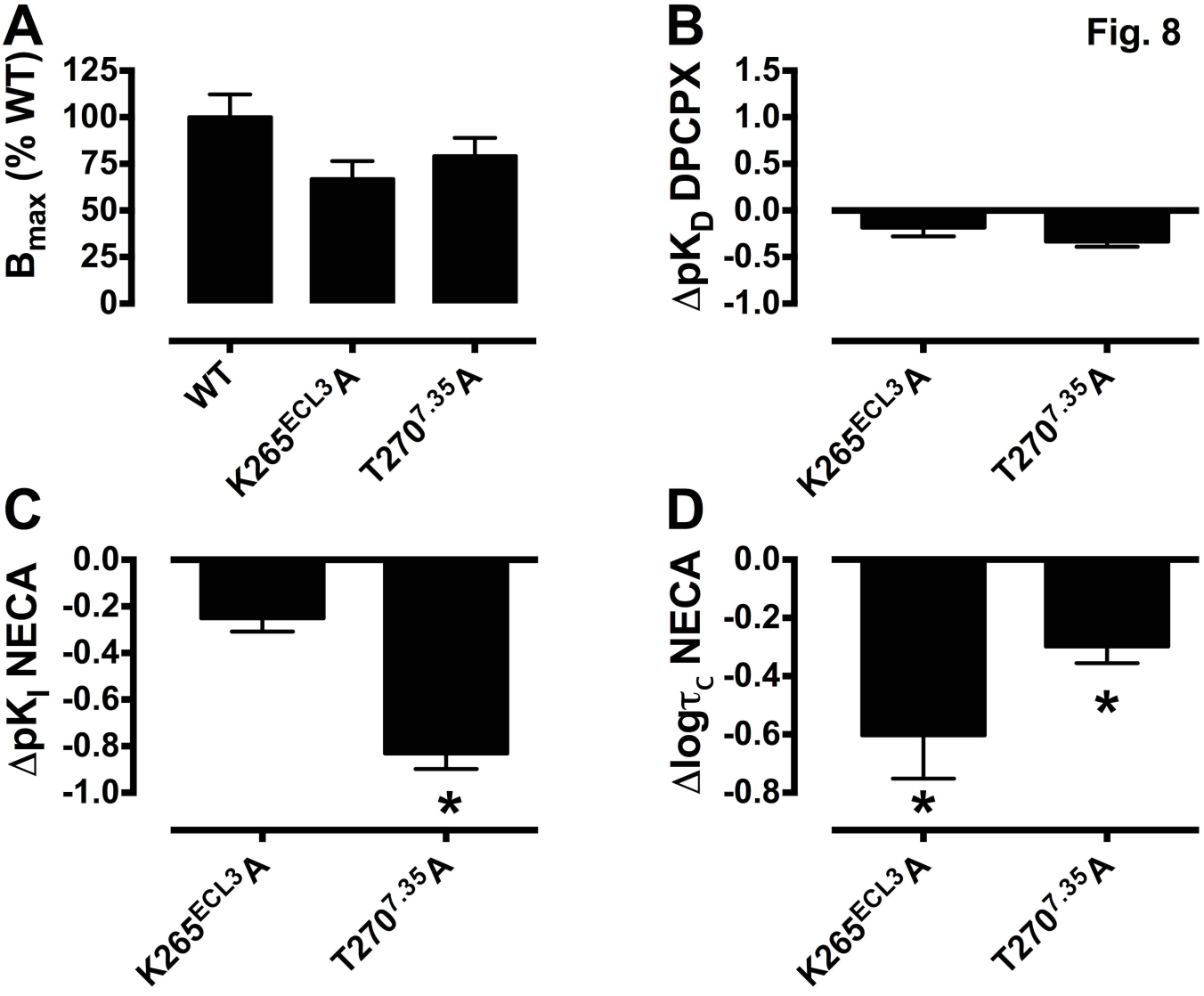
A
B_{max} (% WT)
125
100
75
50
25
0
WT
$K265^{ECL3}A$
$T270^{7.35}A$
B
ΔpK_D DPCPX
1.5
1.0
0.5
0.0
-0.5
-1.0
$K265^{ECL3}A$
$T270^{7.35}A$
C
ΔpK_I NECA
0.0
-0.2
-0.4
-0.6
-0.8
-1.0
*
$K265^{ECL3}A$
$T270^{7.35}A$
D
$\Delta \log \tau_C$ NECA
0.0
-0.2
-0.4
-0.6
-0.8
*
*
$K265^{ECL3}A$
$T270^{7.35}A$